$H_3^+ + H_2$ isotopic system at low temperatures: Microcanonical model and experimental study

Edouard Hugo, Oskar Asvany, and Stephan Schlemmer[a)]
I. Physikalisches Institut, Universität zu Köln, Zülpicher Str. 77, 50937 Köln, Germany

(Received 3 December 2008; accepted 6 February 2009; published online 22 April 2009)

State-to-state thermal rate coefficients for reactions of all $H_3^+ + H_2$ isotopic variants are derived and compared to new experimental data. The theoretical data are also sought for astrochemical modeling of cold environments (<50 K). The rates are calculated on the basis of a microcanonical approach using the Langevin model and the conservation laws of mass, energy, angular momentum, and nuclear spin. Full scrambling of all five nuclei during the collision is assumed for the calculations and alternatively partial dynamical restrictions are considered. The ergodic principle of the collision is employed in two limiting cases, neglecting (weak ergodic limit) or accounting for explicit degeneracies of the reaction mechanisms (strong ergodic limit). The resulting sets of rate coefficients are shown to be consistent with the detailed balance and thermodynamical equilibrium constants. Rate coefficients, $k(T)$, for the deuteration chain of H_3^+ with HD as well as H_2D^+/H_3^+ equilibrium ratios have been measured in a variable temperature 22-pole ion trap. In particular, the $D_2H^+ + HD \rightarrow D_3^+ + H_2$ rate coefficient indicates a change in reaction mechanism when going to higher temperatures. The good overall agreement between experiment and theory encourages the use of the theoretical predictions for astrophysical modeling. © *2009 American Institute of Physics*. [DOI: 10.1063/1.3089422]

I. INTRODUCTION

Deuterium in cold environments such as dense molecular clouds and prestellar or protostellar objects is essentially locked in molecular HD. Yet, many species are observed with deuterium enhancements of several orders of magnitude with respect to the cosmic D/H ratio of 1.5×10^{-5}.[1] Even triply deuterated species are observed.[2,3]

Isotopic substitution, i.e., *X*-H versus *X*-D, is promoted by differences in zero-point vibrational energies (ZPVEs) which can be larger than typical collision energies, $E \sim kT$, thereby favoring the incorporation of deuterium atoms in larger and heavier species. H_3^+ has been identified to play a dominant role in this interstellar relevant isotopic fractionation. H_3^+ originates from cosmic ray ionization of H_2 and a fast exoergic proton transfer reaction with another H_2:

$$H_2 + \zeta \rightarrow H_2^+ + e^-, \tag{1}$$

$$H_2^+ + H_2 \rightarrow H_3^+ + H. \tag{2}$$

It can quickly deuterate in successive steps via exchange or transfer reactions with HD,

$$H_3^+ + HD \rightleftharpoons H_2D^+ + H_2 + \Delta E, \tag{3}$$

$$H_2D^+ + HD \rightleftharpoons D_2H^+ + H_2 + \Delta E, \tag{4}$$

$$D_2H^+ + HD \rightleftharpoons D_3^+ + H_2 + \Delta E, \tag{5}$$

with $\Delta E = 232$, 187, and 234 K for reactions (3)–(5), respectively. One of its deuterium nuclei can then be transferred to "metallic" species via direct reactions such as

$$D_2H^+ + X \rightarrow X\text{-}D^+ + HD, \tag{6}$$

with $X = N_2$, CO, etc. Else, it recombines with a free electron and enriches the medium with free deuterons in reactions such as

$$D_3^+ + e^- \rightarrow D_2 + D \tag{7}$$

$$\rightarrow D + D + D. \tag{8}$$

This may trigger a deuterium-rich ice chemistry after the free deuteron's accretion onto icy grains.[4–6] In this scenario, the H_3^+ cation acts as a vector dragging the deuterium from its reservoir and spreading it further, directly or indirectly, to other species. This pivotal role in the deuterium chemical network is by now well established.

The growing interest of the astronomical community in deuterium chemistry and its H_3^+ parents has been stimulated by numerous detections of deuterated H_3^+,[7–9] leading to ever more complex astrochemical models.[10–16] We now understand that high deuterium fractionations of the H_3^+ cations need not only very low temperatures to occur but also significant depletion of heavy-element-bearing species (CO, N_2) onto the grains and sufficiently low electron abundances. The H_2 *ortho/para* (hereafter o/p) ratio which is thought to be not fully thermalized in dense molecular clouds[17] has also been identified as a limiting factor to the level of deuteration of H_3^+ (Refs. 10 and 18) since, e.g., the 170 K internal energy of o-H_2 ($J=1$) helps overcome the endothermicity of reactions (3)–(5) in the reverse direction.

Regarding theory, the potential energy surface (PES) of the H_5^+ system was first characterized by Yamaguchi *et al.*[19]

a)Electronic mail: schlemmer@ph1.uni-koeln.de.

and has now been explored in greater detail also for its isotopic variants.[20,21] Much of the theoretical work has been concerned with the bond energies and structure of this elusive molecule. Recently, the determination of the vibrational spectrum of H_5^+ is also subject to a number of theoretical work.[22,23]

However, quantum scattering calculations for the $H_3^+ + H_2$ system calculating reactive or inelastic cross sections or rate coefficients are missing to date. Nevertheless, Oka and Epp[24] proposed a simple formulation for the inelastic rate coefficients but their statistical approximation suffers a proper normalization and neglects nuclear spin constraints. More recently, state-to-state rate coefficients including *ortho-para* conversions of the purely hydrogenated system were derived by Park and Light[25] on the basis of a microcanonical statistical approach. Essentially, the present theoretical treatment employs the same statistical approach, where the reaction probability is calculated on the basis of a capture model for the collision considering the cumulative reaction probability (CRP). Complex formation and conservation of the total energy, the total rotational angular momentum, as well as total nuclear spin are used to determine the CRP. In the present study, not only inelastic collisions but, in particular, isotopic reactions are considered.

Prior to the derivation of rate coefficients for the $H_3^+ + H_2$ collision, Quack[26] most imposingly settled the stringent nuclear spin constraints which are at play in reactive collisions. Later, Park and Light[27] carried on those aspects to greater details while Oka[28] gave an elegant reformulation of the selection rules.

In the laboratory, the rate coefficients for all isotopic reactions were first measured with a VT-SIFT apparatus in the temperature range 80–300 K (Refs. 29 and 30) using normal H_2 and normal D_2, i.e., o/p=3 and 2, respectively. Later, Cordonnier *et al.*[31] employed spectroscopic means to analyze nuclear spin reactions of the purely hydrogenated system at temperatures of ~400 K relating *ortho-para* conversion probabilities with reaction mechanisms. More recently, Gerlich *et al.*[18] used a 22-pole ion trap apparatus at 10 K to measure the rate coefficients for reactions (3)–(5) in the forward direction and inferred the speed of reaction (3) in the backward direction by equilibrium measurements in n-H_2 and p-H_2 containing natural impurities of HD. This experimental study demonstrated the detrimental effect of o-H_2 on deuteration for the first time. Nevertheless, the low value for the forward rate coefficients caused a lot of discussion and showed the need for temperature-dependent measurements and theoretical predictions in the low-temperature domain. A recent summary of some of the most important $H_mD_n^+$ collision systems is given in Ref. 32. The branching ratios for some of these systems pose very critical tests to current experimental and theoretical work. In addition, a critical discussion of the *in situ* calibration of HD and the o/p ratio of H_2 and other experimental considerations is given therein.

The $H_3^+ + H_2$ isotopic system represented in Fig. 1 consists of 8 reactions when considering the isotopic exchange between the ionic and neutral collision partner as well as 168 reactions when considering nuclear spin symmetries. Among those reactions, 73 are strictly forbidden assuming nuclear spin conservation (frozen-nuclear spin approximation). Despite the several advances in both theoretical and experimental fields, a complete set of rate coefficients in order to model the interaction of the H_3^+ and H_2 isotopologues in interstellar conditions is still missing and we would like to address this problem here.

Complex	H_3^+		H_2D^+		D_2H^+		D_3^+			ΔZPE > 0	
	ortho	para	ortho	para	para	ortho	para	ortho	meta		
H_5^+	33	0	87	0	50	0	63	43	0	para	H_2
H_4D^+	203	170	257	170	220	170	233	213	170	ortho	
$H_3D_2^+$	265	232	273	187	284	234	63	43	0	HD	
$D_3H_2^+$	372	339	428	341	205	155	63	43	0	ortho	D_2
D_4H^+	457	424	513	426	290	240	148	128	85	para	
D_5^+											

FIG. 1. (Color online) The $H_3^+ + H_2$ isotopic system with nuclear spin details. All reactions within a given isotopic complex (same shade) are possible (i) if allowed by the feasible reaction mechanisms and (ii) if not strictly forbidden by nuclear spin selection rules. The numbers are the channel's zero-point energies ($\Delta E/k$ in Kelvin) relative to their complex' most exoergic channel. The reactions are globally favored in the top right direction.

The paper is organized as follows. In Sec. II, the microcanonical model to calculate thermal state-to-state rate coefficients of the $H_3^+ + H_2$ isotopic system is given. The incorporation of the reaction mechanisms during the complex's lifetime and the ergodic limits are described. The results are presented and analyzed in Sec. III. In Sec. IV, new measurements performed with a 22-pole ion trap apparatus are presented, experimental and theoretical results being compared. Limitations of the current theoretical as well as experimental approach are discussed in the Sec. V. Finally, Sec. VI summarizes the work and draws several conclusions.

II. MICROCANONICAL MODEL

The model is based on phase space theory (PST). It describes the collisions at low temperatures (<50 K) of state specific H_3^+ and H_2 isotopologues. The phase space and the conservation laws are first introduced in Sec. II A by settling the nomenclature and presenting the H_3^+ and H_2 isotopologues. In Sec. II B, we describe the complex formation with the Langevin model and derive statistical weights for nuclear spins and rotational angular momenta from which we obtain reactants-to-complex state-detailed probabilities. Equivalently, the complex decay is treated in Sec. II C specifying statistical weights for mass, nuclear spin, energy, and rotational angular momentum conservation from which complex-to-products state-detailed probabilities are derived. State-to-state cross sections are obtained in Sec. II D by distributing the capture cross section on the basis of the complex formation and decay state-detailed probabilities. State-to-state thermal rate coefficients are derived by integrating the state-to-state cross sections over the Maxwellian collision energy distribution.

TABLE I. Nomenclature of the quantities considered. See the text for detailed explanations.

	Reactants			Products	
	Ion	Neutral		Ion	Neutral
	Motion		Complex	Motion	
Channel	$\mathcal{J}$	$\mathcal{N}$	$\mathcal{C}$	$\mathcal{J}'$	$\mathcal{N}'$
	$\mathcal{M}$			$\mathcal{M}'$	
Mass	m_i	m_n	m_{tot}	$m_{i'}$	$m_{n'}$
	μ			μ'	
Energy	E_i^v	E_n^v	E_{tot}	$E_{i'}^v$	$E_{n'}^v$
	E_i^r	E_n^r		$E_{i'}^r$	$E_{n'}^r$
	E_{col}			E_{col}'	
Rotational angular momentum	J_i	J_n	J_{tot}	$J_{i'}$	$J_{n'}$
	l			l'	
Nuclear spin symmetry	Γ_i^{H}	Γ_n^{H}	$\Gamma_{\text{tot}}^{\text{H}}$	$\Gamma_{i'}^{\text{H}}$	$\Gamma_{n'}^{\text{H}}$
	Γ_i^{D}	Γ_n^{D}	$\Gamma_{\text{tot}}^{\text{D}}$	$\Gamma_{i'}^{\text{D}}$	$\Gamma_{n'}^{\text{D}}$
Polarizability and charge		α_n			$\alpha_{n'}$
	q_i			$q_{i'}$	

A. Phase space and conservation laws

1. Microstates and phase space

The reaction process is decomposed in the entrance channel ($\mathcal{JNM}$), the complex channel $\mathcal{C}$, and the exit channel ($\mathcal{J}'\mathcal{N}'\mathcal{M}'$). The internal states (microstates) of the reactants, intermediate complexes, and products are expressed in the phase space consisting of mass and energy scalars as well as rotational angular momentum and nuclear spin vectors. The entrance channel consists in an ion $\mathcal{J}$, a neutral $\mathcal{N}$, and their relative motional channel $\mathcal{M}$. An ion $\mathcal{J}$ or a neutral $\mathcal{N}$ is defined by its degree of isotopic substitution determining its mass m and ZPVE E^v, its nuclear spin symmetries for hydrogen nuclei Γ^{H} and deuterium nuclei Γ^{D}, and its rotational state described by rotational quantum number(s)—among which the rotational angular momentum J—determining its rotational energy E^r. The charge of the ion is q_i, and the isotropic polarizability of the neutral is α_n. The subscripts i and n are used to define the quantities of the ion and the neutral, respectively. A relative motion $\mathcal{M}$ is described by the collision energy E_{col} and the quantum orbital angular momentum l. The reduced mass of two species is denoted as μ. The exit channel ($\mathcal{J}'\mathcal{N}'\mathcal{M}'$) and its quantities are defined identically and referred to with a prime. The intermediate complex channel $\mathcal{C}$ is defined by its total mass m_{tot}, total energy E_{tot}, total rotational angular momentum J_{tot}, and total nuclear spin symmetries for hydrogen nuclei $\Gamma_{\text{tot}}^{\text{H}}$ and deuterium nuclei $\Gamma_{\text{tot}}^{\text{D}}$. Table I summarizes the quantities used in this paper.

Table II details the channels for the ions and the neutrals which were considered in the following calculations. The rotational states of the species correlate with the nuclear spin symmetry representations according to the symmetrization postulate.[35] As first introduced by Maue[36] for methane, the Greek appellations *ortho*, *meta*, and *para* for the different nuclear spin symmetry representations Γ_i (i.e., modifications) of an isotopologue are assigned in decreasing order of their high-temperature ($T \to \infty$) statistical weights $W_{(\Gamma_i)}^{\infty}$ which is simply their high-temperature populations. The $W_{(\Gamma_i)}^{\infty}$ are thus proportional to their total number of rovibronic states $N_{\text{rve}}(\Gamma_i)$ and the nuclear spin degeneracy of their rovibronic states $g(\Gamma_i)$:

$$W_{(\Gamma_i)}^{\infty} = g(\Gamma_i) \times N_{\text{rve}}(\Gamma_i). \tag{9}$$

Since $g(\Gamma_i)$ is the frequency of the representation, $f(\Gamma_i)$, and $N_{\text{rve}}(\Gamma_i)$ is proportional to its dimension $\dim(\Gamma_i)$,

$$g(\Gamma_i) = f(\Gamma_i), \tag{10}$$

$$\frac{N_{\text{rve}}(\Gamma_i)}{\dim(\Gamma_i)} = \frac{N_{\text{rve}}(\Gamma_j)}{\dim(\Gamma_j)}, \tag{11}$$

the high-temperature statistical weight of a nuclear spin symmetry representation is proportional to its frequency and its dimension, i.e., its pure nuclear spin statistical weight,

$$\frac{W_{(\Gamma_i)}^{\infty}}{W_{(\Gamma_j)}^{\infty}} = \frac{f(\Gamma_i) \times \dim(\Gamma_i)}{f(\Gamma_j) \times \dim(\Gamma_j)}. \tag{12}$$

It is noteworthy that in the literature, the appellations for the nuclear spin modifications are often misassigned in decreasing order of the rovibronic state's nuclear spin degeneracy $g(\Gamma_i)$ only, neglecting the nuclear spin representation's total number of rovibronic states $N_{\text{rve}}(\Gamma_i)$. This results in the exchange of *ortho* and *meta* appellations for D_3^+ (Refs. 15, 37, and 38) and could lead to confusions and errors.

The ZPVEs[33,34] in Table II are expressed relative to D_3^+ for the ions and D_2 for the neutrals. Only the vibronic ground states were considered according to the low temperatures of interest. The rotational energies of H_2, HD, and D_2 were calculated according to Ramanlal and Tennyson.[34] The rotational energies of H_3^+ were taken from Lindsay and McCall,[39] those of H_2D^+ and D_2H^+ were taken from Tennyson.[40] For the D_3^+ rotational levels, we used the parameters for the

TABLE II. H_3^+ and H_2 isotopologues: mass, ZPVE, nuclear spin symmetries, and lowest rotational levels.

Isotopologue	H_2D^+		D_2H^+		D_3^+		
Mass (amu)	4		5		6		
ZPVE[a] (K)	1245.8		646.2		0		
Modification[b]	*ortho* (9)	*para* (3)	*ortho* (12)	*para* (6)	*ortho* (16)	*meta* (10)	*para* (1)
H symmetry[c]	3 *A* (1)	1 *B* (1)	2 *A* (1)	2 *A* (1)			
D symmetry[c]	3 *A* (1)	3 *A* (1)	6 *A* (1)	3 *B* (1)	8 *E* (2)	10 A_1 (1)	1 A_2 (1)
Selection rules[d]	K_a odd	K_a even	K_a+K_c even	K_a+K_c odd	$K=3n\pm1$	$K=0$, J even or $K=3n$	$K=0$, J odd or $K=3n$
Rotational levels[e]	86.4 (1_{11})	0.0 (0_{00})	0.0 (0_{00})	50.2 (1_{01})	46.5 (1_1)	0.0 (0_0)	62.7 (1_0)
	104.2 (1_{10})	65.8 (1_{01})	70.9 (1_{11})	83.4 (1_{10})	123.2 (2_2)	187.9 (2_0)	230.0 (3_3)
	199.8 (2_{12})	189.4 (2_{02})	146.3 (2_{02})	158.6 (2_{12})	171.7 (2_1)	230.0 (3_3)	374.7 (3_0)
	253.1 (2_{11})	314.6 (2_{21})	196.2 (2_{11})	257.8 (2_{21})	310.6 (3_2)	622.3 (4_0)	730.6 (6_6)
	365.5 (3_{13})	322.1 (2_{20})	262.0 (2_{20})	282.1 (3_{03})	358.7 (3_1)	730.6 (6_6)	788.4 (5_3)
	469.3 (3_{12})	361.7 (3_{03})	287.8 (3_{13})	361.6 (3_{12})	366.9 (4_4)	788.4 (5_3)	929.1 (5_0)
	580.7 (4_{14})	510.4 (3_{22})	407.7 (3_{22})	426.0 (3_{21})	533.8 (5_5)	1155.6 (6_3)	1155.6 (6_3)
	659.5 (3_{31})	541.5 (3_{21})	554.3 (4_{04})	456.4 (4_{14})	559.0 (4_2)	1163.1 (7_6)	1163.1 (7_6)
	661.6 (3_{30})	579.6 (4_{04})	542.6 (3_{31})	543.5 (3_{30})	606.5 (4_1)	1293.5 (6_0)	1499.0 (9_9)

Isotopologue	H_3^+		H_2		HD	D_2	
Mass (amu)	3		2		3	4	
ZPVE[a] (K)	1797.7		903.6		491.2	0	
Modification[b]	*ortho* (4)	*para* (4)	*ortho* (3)	*para* (1)	(6)	*ortho* (6)	*para* (3)
H symmetry[c]	4 A_1 (1)	2 *E* (2)	3 *A* (1)	1 *B* (1)	2 *A* (1)		
D symmetry[c]					3 *A* (1)	6 *A* (1)	3 *B* (1)
Selection rules[d]	$K=0$, J odd or $K=3n$	$K=3n\pm1$	J odd	J even		J even	J odd
Rotational levels[e]	125.1 (1_0)	92.3 (1_1)	170.4 (1)	0.0 (0)	0.0 (0)	0.0 (0)	85.9 (1)
	453.7 (3_3)	243.6 (2_2)	1014.5 (3)	509.7 (2)	128.4 (1)	257.6 (2)	513.9 (3)
	743.7 (3_0)	341.5 (2_1)	2499.6 (5)	1679.9 (4)	384.2 (2)	853.9 (4)	1276.0 (5)
	947.7 (4_3)	615.8 (3_2)	4567.2 (7)	3465.3 (6)	765.7 (3)	1778.1 (6)	2357.9 (7)
	1432.8 (6_6)	711.8 (3_1)					
	1554.5 (5_3)	722.3 (4_4)					
	1829.0 (5_0)	1048.9 (5_5)					
	2269.4 (6_3)	1105.6 (4_2)					
	2282.7 (7_6)	1199.3 (4_1)					

[a]Relative to the ZPVE of D_3^+ and D_2 (Refs. 33 and 34).
[b]The integer in parenthesis represents the high-temperature statistical weight, i.e., the pure nuclear spin statistical weight, as defined in Eq. (12).
[c]Symmetry representation in the appropriate permutation group. The first integer is the frequency of the representation, i.e., the nuclear spin degeneracy of the rovibronic states, and the integer in parenthesis is the dimension, i.e., the density of rovibronic states.
[d]Rotational selection rules for the vibronic ground states according to the symmetrization postulate.
[e]Energies in Kelvin and quantum numbers in parenthesis: J for H_2, HD, and D_2, J_K for H_3^+ and D_3^+, and $J_{K_aK_c}$ for H_2D^+ and D_2H^+.

Watson Hamiltonian given by Miller and Tennyson.[41] All energies were rounded with 0.1 K accuracy. In order to avoid errors due to energy truncation for the low-lying states of interest, we systematically included the nine and four lowest levels of each H_3^+ and H_2 isotopologue and modification. The isotropic polarizability of H_2, HD, and D_2 was taken as 0.79 Å^3.[42]

2. Conservation laws

The phase space volume in which a given microstate can evolve is restricted by the conservation of the total mass, total energy, total rotational angular momentum, and hydrogen and deuterium total nuclear spin symmetries:

$$m_i + m_n = m_{\text{tot}} = m_{i'} + m_{n'}, \tag{13}$$

$$E_i^v + E_i^r + E_n^v + E_n^r + E_{\text{col}} = E_{\text{tot}} = E_{i'}^v + E_{i'}^r + E_{n'}^v + E_{n'}^r + E_{\text{col}'}, \tag{14}$$

$$J_i \otimes J_n \otimes l \uparrow J_{\text{tot}} \downarrow J_{i'} \otimes J_{n'} \otimes l', \tag{15}$$

$$\Gamma_i^{\text{H}} \otimes \Gamma_n^{\text{H}} \uparrow \Gamma_{\text{tot}}^{\text{H}} \downarrow \Gamma_{i'}^{\text{H}} \otimes \Gamma_{n'}^{\text{H}}, \tag{16}$$

$$\Gamma_i^D \otimes \Gamma_n^D \uparrow \Gamma_{tot}^D \downarrow \Gamma_{i'}^D \otimes \Gamma_{n'}^D. \quad (17)$$

Equation (13) is equivalent to the conservation of the hydrogen and deuterium nuclei. The $\otimes$ operators in Eq. (15) and Eqs. (16) and (17) are the direct products for the K spatial rotation group (i.e., vectorial sum of angular momenta) and the nuclear permutation groups, respectively. The $\uparrow$ and $\downarrow$ operators correspond to inductions and subductions of the representations in the groups of concern.[26,28] The nuclear spins are treated as completely decoupled from the other degrees of freedom considering the lack of significant magnetic couplings during the collision process.[27,43] The nuclear spins are thus assumed to be frozen, resulting in the strict conservation of the total spin angular momenta, symmetries, and magnetic moments. The constraints and statistics rising from this *frozen-nuclear spin* approximation have already been discussed in the literature regarding symmetry,[26] angular momentum,[27] or both.[28] Regarding the symmetrization postulate, the nuclear spin symmetry representations must be considered contrarily to their angular momentum representations. Total parity conservation was not considered in the present calculations.

Transition probabilities of the microstates are assumed to fulfill the equiprobability principle according to the ergodic principle and the full-scrambling hypothesis inferred from the topology of the H_5^+ PES (see Sec. II E). Throughout this paper, the weights and probabilities derived according to those conservation laws will be written with the general form $W_{(\beta|\alpha)}$ and $P_{(\beta|\alpha)}$ with α and β being the prior and posterior informations.

B. Complex formation

Consider a given entrance channel ($\mathcal{JN}$) representing two H_3^+ and H_2 isotopologues with specific internal states.

1. Langevin model

Let the two reactants be on a trajectory with a collision energy E_{col} and an impact parameter b corresponding to a motional channel $\mathcal{M}$. The reduced mass of the ion-neutral reacting system is

$$\mu = \frac{m_i \times m_n}{m_i + m_n}. \quad (18)$$

Their relative motion may be described by the classical Langevin model. Considering the charge-induced dipole interaction and the centrifugal energy of the orbital motion, the long-range effective potential between the reactants in Joules is

$$V_{eff}(r) = -\frac{1}{2}\frac{1}{4\pi\epsilon_0}\frac{q_i^2\alpha_n}{r^4} + E_{col}\left(\frac{b}{r}\right)^2, \quad (19)$$

r being the distance between the reactants in meters, q the charge of the ion in Coulombs, α the isotropic polarizability of the neutral in m^3, E_{col} the collision energy in Joules, and b the impact parameter in meters. Taking as a capture criterium the condition that the collision energy is sufficient to overcome the barrier of the effective potential ($E_{col} > V_{eff}^{max}$) leads to a critical impact parameter b_c given by

$$b_c^2 = \sqrt{\frac{q_i^2\alpha_n}{2\pi\epsilon_0 E_{col}}} \quad (20)$$

and the Langevin capture cross section

$$\sigma_c(E_{col}) = \pi b_c^2. \quad (21)$$

For a given collision energy, it is assumed that a complex with a finite lifetime is formed if the impact parameter is below this critical value; else no complex is formed. The complex lifetimes are considered to be much longer than any period of an internal motion. This is taken as a justification to use a phase space approach for calculating the reaction probabilities and subsequently also the cross sections. In contrast, direct transitions[44] which might result from distant trajectories ($b > b_c$) are neglected as well as radiative association processes.

The classical orbital angular momentum L of the collision is given by $L^2 = 2\mu b^2 E_{col}$ and is related to the quantum orbital angular momentum l by $L^2 = l(l+1)\hbar^2$. The maximum classical orbital angular momentum L_{max} and the maximum quantum orbital angular momentum l_{max} for the formation of a complex are thus given by

$$2\mu b_c^2 E_{col} = L_{max}^2 \equiv l_{max}(l_{max}+1)\hbar^2, \quad (22)$$

$$l_{max}(l_{max}+1) \leqslant \frac{L_{max}^2}{\hbar^2} \leqslant (l_{max}+1)(l_{max}+2). \quad (23)$$

Equation (23) discretizes the classical picture. It results that the quantum orbital angular momentum l for a given collision energy E_{col} can have equiprobable values in the range $0 \leqslant l \leqslant l_{max}$, that is,

$$W_{(l|\mu,E_{col})} = \begin{cases} 1 & \text{if } l \leqslant l_{max} \\ 0 & \text{if } l > l_{max}. \end{cases} \quad (24)$$

The charge of the ion and the polarizability of the neutral are not explicited here since they are the same for all isotoplogs but they are implicitly contained in l_{max}. This equation corresponds to the heavyside transmission function of Park and Light [see Ref. 25, Eq. (43)] where the transmission between a complex and reactants with a given orbital angular momentum is constrained by the minimum collision energy necessary, i.e., $E_{col} > V_{eff}^{max}$, while in our case, the transmission between a complex and reactants with a given collision energy is constrained by the maximum orbital angular momentum feasible defined with the condition $V_{eff}^{max} < E_{col}$.

2. Angular momentum conservation

The vectorial sum of the three rotational angular momenta J_i, J_n, and l induces a total rotational angular momentum J_{tot} as described by the first part of Eq. (15). Its statistical weight, as derived with angular momentum algebra, is

$$W_{(J_{\text{tot}}|J_i,J_n,l)} = (2J_{\text{tot}}+1)\sum_{J_{in}=|J_i-J_n|}^{J_i+J_n}\sum_{J_{inl}=|J_{in}-l|}^{J_{in}+l}\delta_{J_{\text{tot}}J_{inl}}, \tag{25}$$

$\delta_{J_{\text{tot}}J_{inl}}$ being the Kronecker delta. Given a collision energy, the statistical weight of a total rotational angular momentum is the sum of the previous weight over all possible motional channels $\mathcal{M}$, i.e., orbital angular momenta:

$$W_{(J_{\text{tot}}|J_i,J_n,\mu,E_{\text{col}})} = \sum_{l=0}^{\infty} W_{(J_{\text{tot}}|J_i,J_n,l)} \times W_{(l|\mu,E_{\text{col}})} = \sum_{l=0}^{l_{\max}} W_{(J_{\text{tot}}|J_i,J_n,l)}, \tag{26}$$

$l_{\max}$ being the maximum orbital angular momentum defined in Eq. (23).

3. Nuclear spin conservation

The hydrogen and deuterium nuclei must be considered separately since they are distinguishable. The direct product of the local nuclear spin symmetries Γ_i and Γ_n induces a total nuclear spin symmetry Γ_{tot} as decribed by the first part of Eqs. (16) and (17) for hydrogen and deuterium nuclei, and their pure nuclear spin statistical weights are given in Tables III and IV, respectively. These weights can be derived from the work of Quack,[26], Park and Light,[27] as well as, Oka[28], yet a more explicit method will be given in a forthcoming publication. They are directly used in the microcanonical model,

$$W_{(\Gamma_{\text{tot}}|\Gamma_i,\Gamma_n)} = W_{(\Gamma_i\otimes\Gamma_n\uparrow\Gamma_{\text{tot}})}. \tag{27}$$

It is noteworthy that, according to the Frobenius reciprocity principle, the statistical weight of an induction and its reciprocal subduction are equal,

$$W_{(\Gamma_i\otimes\Gamma_n\uparrow\Gamma_{\text{tot}})} = W_{(\Gamma_{\text{tot}}\downarrow\Gamma_i\otimes\Gamma_n)}. \tag{28}$$

In the case of an o-H_2D^++HD$\rightarrow H_3D_2^+$ collision, the hydrogen and deuterium components are

$$\frac{\text{o-H}_2+\text{H}\rightarrow\text{H}_3}{S_2\otimes S_1\uparrow S_3}, \quad A\otimes A\uparrow\Gamma_{\text{tot}}^{\text{H}}$$

$$\frac{\text{D}+\text{D}\rightarrow\text{D}_2}{S_1\otimes S_1\uparrow S_2}, \quad A\otimes A\uparrow\Gamma_{\text{tot}}^{\text{D}}$$

S_n being the permutation group of n identical nuclei. The statistical weights for $\Gamma_{\text{tot}}^{\text{H}}$ and $\Gamma_{\text{tot}}^{\text{D}}$ are

$$W_{(\Gamma_{\text{tot}}^{\text{H}}|\Gamma_i^{\text{H}}=A,\Gamma_n^{\text{H}}=A)} = \begin{cases} 4 & \text{for } \Gamma_{\text{tot}}^{\text{H}} = A_1 \\ 2 & \text{for } \Gamma_{\text{tot}}^{\text{H}} = E \end{cases}, \tag{29}$$

$$W_{(\Gamma_{\text{tot}}^{\text{D}}|\Gamma_i^{\text{D}}=A,\Gamma_n^{\text{D}}=A)} = \begin{cases} 6 & \text{for } \Gamma_{\text{tot}}^{\text{D}} = A \\ 3 & \text{for } \Gamma_{\text{tot}}^{\text{D}} = B \end{cases}. \tag{30}$$

TABLE III. Pure nuclear spin symmetry induction and subduction statistical weights, $W_{(\Gamma_i\otimes\Gamma_n\uparrow\Gamma_{\text{tot}})}=W_{(\Gamma_{\text{tot}}\downarrow\Gamma_i\otimes\Gamma_n)}$, for several hydrogen systems.

$H+H\rightarrow H_2$

		A	B	Total
A	A	3	1	4
Total		3	1	$4=2^2$

$H_2+H\rightarrow H_3$

		A_1	A_2	E	Total
A	A	4	0	2	6
B	A	0	0	2	2
Total		4	0	4	$8=2^3$

$H_3+H\rightarrow H_4$

		A_1	A_2	E	F_1 [a]	F_2 [a]	Total
A_1	A	5	0	0	3	0	8
A_2	A	0	0	0	0	0	0
E	A	0	0	2	6	0	8
Total		5	0	2	9	0	$16=2^4$

$H_2+H_2\rightarrow H_4$

		A_1	A_2	E	F_1 [a]	F_2 [a]	Total
A	A	5	0	1	3	0	8
A	B	0	0	0	3	0	0
B	A	0	0	0	3	0	8
B	B	0	0	1	0	0	8
Total		5	0	2	9	0	$16=2^4$

$H_3+H_2\rightarrow H_5$

		A_1	A_2	G_1	G_2	H_1	H_2	I	Total
A_1	A	6	0	4	0	2	0	0	12
A_1	B	0	0	4	0	0	0	0	4
A_2	A	0	0	0	0	0	0	0	0
A_2	B	0	0	0	0	0	0	0	0
E	A	0	0	8	0	4	0	0	12
E	B	0	0	0	0	4	0	0	4
Total		6	0	16	0	10	0	0	$32=2^5$

[a]The symmetry labels F_1 and F_2 of S_4 are inverted with respect to Refs. 26 and 27.

In the case of a m-D_3^++p-$H_2\rightarrow D_3H_2^+$ collision, the total hydrogen and deuterium symmetries are simply the local symmetries of the neutral and ion reactants with statistical weights

$$W_{(\Gamma_{\text{tot}}^{\text{H}}=B|\Gamma_i^{\text{H}}=\varnothing,\Gamma_n^{\text{H}}=\text{B})} = 1, \tag{31}$$

$$W_{(\Gamma_{\text{tot}}^{\text{D}}=A_1|\Gamma_i^{\text{D}}=A_1,\Gamma_n^{\text{D}}=\varnothing)} = 10. \tag{32}$$

4. Overall complex formation probability

The total mass m_{tot} and total energy E_{tot} of the formed complex are given by the first parts of Eqs. (13) and (14). For the total rotational angular momentum J_{tot} and the total hydrogen and deuterium nuclear spin symetries $\Gamma_{\text{tot}}^{\text{H}}$ and $\Gamma_{\text{tot}}^{\text{D}}$, the overall weight of a complex channel $\mathcal{C}$ given a reactant channel $(\mathcal{JN})$ and a collision energy E_{col} is

TABLE IV. Pure nuclear spin symmetry induction and subduction statistical weights, $W_{(\Gamma_i \otimes \Gamma_n \uparrow \Gamma_{tot})} = W_{(\Gamma_{tot} \downarrow \Gamma_i \otimes \Gamma_n)}$, for several deuterium systems.

$D+D \rightarrow D_2$

		A	B	Total
A	A	6	3	9
Total		6	3	$9=3^2$

$D_2+D \rightarrow D_3$

		A_1	A_2	E	Total
A	A	10	0	8	18
B	A	0	1	8	9
Total		10	1	16	$27=3^3$

$D_3+D \rightarrow D_4$

		A_1	A_2	E	F_1 [a]	F_2 [a]	Total
A_2	A	15	0	0	15	0	30
A_2	A	0	0	0	0	3	3
E	A	0	0	12	30	6	48
Total		15	0	12	45	9	$81=3^4$

$D_2+D_2 \rightarrow D_4$

		A_1	A_2	E	F_1 [a]	F_2 [a]	Total
A	A	15	0	6	15	0	36
A	B	0	0	0	15	3	18
B	A	0	0	0	15	3	18
B	B	0	0	6	0	3	9
Total		15	0	12	45	9	$81=3^4$

$D_3+D_2 \rightarrow D_5$

		A_1	A_2	G_1	G_2	H_1	H_2	I	Total
A_1	A	21	0	24	0	15	0	0	60
A_1	B	0	0	24	0	0	0	6	30
A_2	A	0	0	0	0	0	0	6	6
A_2	B	0	0	0	0	0	3	0	3
E	A	0	0	48	0	30	6	12	96
E	B	0	0	0	0	30	6	12	48
Total		21	0	96	0	75	15	36	$243=3^5$

[a]The symmetry labels F_1 and F_2 of S_4 are inverted with respect to Refs. 26 and 27.

$$W_{(\mathcal{C}|\mathcal{J},\mathcal{N},E_{col})} = W_{(J_{tot}|J_i,J_n,\mu,E_{col})} \times W_{(\Gamma^H_{tot}|\Gamma^H_i,\Gamma^H_n)} \times W_{(\Gamma^D_{tot}|\Gamma^D_i,\Gamma^D_n)} \quad (33)$$

and its overall probability is

$$P_{(\mathcal{C}|\mathcal{J},\mathcal{N},E_{col})} = \frac{W_{(\mathcal{C}|\mathcal{J},\mathcal{N},E_{col})}}{\Sigma_{\mathcal{C}} W_{(\mathcal{C}|\mathcal{J},\mathcal{N},E_{col})}}. \quad (34)$$

C. Complex decay

Consider a given complex channel $\mathcal{C}$ with a total mass m_{tot}, total energy E_{tot}, total rotational angular momentum J_{tot}, and total nuclear spin symmetries Γ^H_{tot} and Γ^D_{tot} for its hydrogen and deuterium nuclei.

TABLE V. Microcanonical isotopic statistical weights of $H_2D^+ + HD$ collisions for the full-scrambling and hop limits as used in sec. II C 1. The accessible dissociative asymptotes correspond to reaction mechanisms for which the hydrogen and/or deuterium nuclei involved are specified.

	Reaction mechanisms			
Isotopic channel	Identity	Transfer	Exchange	Total[a]
Full-scrambling limit				
$H_3^+ + D_2$	0	0	1 D-H	1 (1)
$H_2D^+ + HD$	1	2 H	2 H-H	6 (1)
			1 D-D	
$D_2H^+ + H_2$	0	1 D	2 H-D	3 (1)
Total	1	3	6	10
Hop limit				
H nucleus locked in the center: Probability 2/3				
$H_3^+ + D_2$	0	0	0	0 (0)
$H_2D^+ + HD$	1	1 H	0	2 (1)
$D_2H^+ + H_2$	0	0	0	0 (0)
Total	1	1	0	2
D nucleus locked in the center: Probability 1/3				
$H_3^+ + D_2$	0	0	0	0 (0)
$H_2D^+ + HD$	1	0	0	1 (1)
$D_2H^+ + H_2$	0	1 D	0	1 (1)
Total	1	1	0	2

[a]Isotopic statistical weight for the strong ergodic limit. The number in parenthesis corresponds to the weak ergodic limit which only accounts for the accessibility of the channel.

1. Mass conservation

The accessible isotopic channels $(m_{i'}, m_{n'})$ are constrained by the second equality of Eq. (13) and the feasible reaction mechanisms. In the most simple approach corresponding to the full-scrambling hypothesis and the weak ergodic limit (see Sec. II E and Table V), the weights are

$$W_{(m_{i'},m_{n'}|m_{tot})} = \begin{cases} 1 & \text{if } m_{i'} + m_{n'} = m_{tot} \\ 0 & \text{else} \end{cases}. \quad (35)$$

As an example, a $D_3H_2^+$ complex can decay to the following isotopic channels:

$$D_3H_2^+ \rightarrow H_2D^+ + D_2$$
$$\rightarrow D_2H^+ + HD$$
$$\rightarrow D_3^+ + H_2.$$

According to Eq. (35), all possible isotopic channels are considered with equal probability. However, as will be discussed below, different weights may be introduced accounting for accessible and inaccessible dissociative asymptotes of the different product isotopologues. Therefore reaction mechanism degeneracies have to be accounted for. The introduction of these weights is moved to the end of this section in order to proceed with the overall derivation of the desired state-to-state rate coefficients.

2. Nuclear spin conservation

Within a given isotopic channel, the accessible nuclear spin channels are constrained by the subduction parts of Eqs. (16) and (17) and the feasible reaction mechanisms.[28] According to the Frobenius reciprocity principle, the statistical weights for the induction and subduction of a total symmetry Γ_{tot} for both hydrogen and deuterium nuclei are equal as stated in Eq. (28). However, since the rotational states correlate with the nuclear spin symmetries as pointed out in Sec. II A 1, the full-scrambling statistical weight of the products' local symmetries $\Gamma_{i'}$ and $\Gamma_{n'}$ emerging from a total symmetry Γ_{tot} for both hydrogen and deuterium nuclei are taken as

$$W_{(\Gamma_{i'},\Gamma_{n'}|\Gamma_{\text{tot}})} = \frac{W_{(\Gamma_{\text{tot}}\downarrow\Gamma_{i'}\otimes\Gamma_{n'})}}{\dim(\Gamma_{i'})\times\dim(\Gamma_{n'})}, \tag{36}$$

where the numerator is the pure nuclear spin subduction statistical weight given in Tables III and IV and the denominators are the dimensions of the products' nuclear spin representations given in Table II.

In the case of a D_4H^+ complex with $\Gamma_{\text{tot}}^{\text{D}}=F_2$, the accessible and inaccessible isotopic and nuclear spin channels are

$$\begin{aligned} D_4H^+(\Gamma_{\text{tot}}^{\text{D}}=F_2) \quad &\rightarrow o\text{-}D_2H^+ + p\text{-}D_2 \\ &\quad\; p\text{-}D_2H^+ + o\text{-}D_2 \\ &\quad\; p\text{-}D_2H^+ + p\text{-}D_2 \\ &\nrightarrow o\text{-}D_2H^+ + o\text{-}D_2 \\ &\rightarrow o\text{-}D_3^+ + HD \\ &\quad\; p\text{-}D_3^+ + HD \\ &\nrightarrow m\text{-}D_3^+ + HD, \end{aligned}$$

with the deuterium nuclear spin statistical weights of, i.e., the D_3^++HD isotopic channel

$$W_{(E,A|F_2)} = 3, \tag{37}$$

$$W_{(A_2,A|F_2)} = 3, \tag{38}$$

$$W_{(A_1,A|F_2)} = 0. \tag{39}$$

Note that Eq. (36) ensures that the high-temperature statistics are consistent with the pure nuclear spin statistics. Indeed, in the high-temperature limit (i.e., infinite energy and orbital angular momentum), all the internal states of an isotopic channel are accessible irrespective of their energy and rotational angular momentum such that

$$\begin{aligned} W^{\infty}_{(\Gamma_{i'},\Gamma_{n'}|\Gamma_{\text{tot}})} &\propto \sum_{\mathcal{J}'\in\Gamma_{i'}}\sum_{\mathcal{N}'\in\Gamma_{n'}} W_{(\Gamma_{i'},\Gamma_{n'}|\Gamma_{\text{tot}})} \\ &\propto N_{\text{rve}}(\Gamma_{i'})\times N_{\text{rve}}(\Gamma_{n'})\times W_{(\Gamma_{i'},\Gamma_{n'}|\Gamma_{\text{tot}})} \end{aligned} \tag{40}$$

and given Eq. (11), we find

$$\begin{aligned} W^{\infty}_{(\Gamma_{i'},\Gamma_{n'}|\Gamma_{\text{tot}})} &\propto \dim(\Gamma_{i'})\times\dim(\Gamma_{n'})\times W_{(\Gamma_{i'},\Gamma_{n'}|\Gamma_{\text{tot}})} \\ &\propto W_{(\Gamma_{\text{tot}}\downarrow\Gamma_{i'}\otimes\Gamma_{n'})}. \end{aligned} \tag{41}$$

Regarding the previous example, the ratios of the high-temperature statistical weights of the nuclear spin channels of D_3^++HD are

$$W^{\infty}_{(A_1|F_2)}:W^{\infty}_{(A_2|F_2)}:W^{\infty}_{(E|F_2)} = 0:3:6, \tag{42}$$

which agrees as expected with the deuterium statistical weights of D_3^++D emerging from $\Gamma_{\text{tot}}^{\text{D}}=F_2$ (see Table IV).

3. Energy conservation

Within a given isotopic and nuclear spin channel, the accessible rotational channels are constrained by the second equality of Eq. (14). A rotational channel with its vibrational and rotational energies $E^{v}_{i'}$, $E^{r}_{i'}$, $E^{v}_{n'}$, and $E^{r}_{n'}$ may only be accessed if the complex has enough total energy which we can translate with the energy statistical weight[45]

$$W_{(E^{v}_{i'},E^{r}_{i'},E^{v}_{n'},E^{r}_{n'}|E_{\text{tot}})} = \begin{cases} 1 & \text{if } E_{\text{col}'} \geqslant 0 \\ 0 & \text{else,} \end{cases} \tag{43}$$

with $E_{\text{col}'}=E_{\text{tot}}-E^{v}_{i'}+E^{r}_{i'}+E^{v}_{n'}+E^{r}_{n'}$ the relative kinetic energy of the products' motional channel.

4. Angular momentum conservation

Moreover, only the motional channels $\mathcal{M}'$ whose kinetic energy is superior to the maximum of the effective potential of the exit channel are accessible. Conversely, the barrier of the effective potential should be lower than the products' relative kinetic energy ($V^{\max}_{\text{eff}'}<E_{\text{col}'}$). As developed in Sec. II B 1, this condition leads to the statistical weight

$$W_{(l'|\mu',E_{\text{col}'})} = \begin{cases} 1 & \text{if } l' \leqslant l'_{\max} \\ 0 & \text{if } l' > l'_{\max}, \end{cases} \tag{44}$$

with $l'_{\max}$ defined as in Eq. (23).

The rotational angular momentum statistical weight of a product channel $(\mathcal{J}'\mathcal{N}')$ is obtained by summing over all accessible motional channels $\mathcal{M}'$, i.e., orbital angular momenta l':

$$W_{(J_{i'},J_{n'},\mu',E_{\text{col}'}|J_{\text{tot}})} = \sum_{l'=0}^{l'_{\max}} W_{(J_{i'},J_{n'},l'|J_{\text{tot}})}, \tag{45}$$

where $W_{(J_{i'},J_{n'},l'|J_{\text{tot}})}$ is the statistical weight of an angular momentum channel $(J_{i'},J_{n'},l')$ given a total rotational angular momentum J_{tot}. This weight describing the subduction part of Eq. (15) can be straightforwardly inferred from its reciprocal induction [Eq. (25)] using the Frobenius reciprocity principle:

$$W_{(J_{i'},J_{n'},l'|J_{\text{tot}})} = W_{(J_{\text{tot}}|J_{i'},J_{n'},l')}. \tag{46}$$

5. Overall decay probability

The overall weight of a product channel $(\mathcal{J}'\mathcal{N}')$ given a complex channel $\mathcal{C}$ is

$$\begin{aligned} W_{(\mathcal{J}',\mathcal{N}'|\mathcal{C})} = W_{(m_{i'},m_{n'}|m_{\text{tot}})} &\times W_{(\Gamma^{\text{H}}_{i'},\Gamma^{\text{H}}_{n'}|\Gamma^{\text{H}}_{\text{tot}})}\times W_{(\Gamma^{\text{D}}_{i'},\Gamma^{\text{D}}_{n'}|\Gamma^{\text{D}}_{\text{tot}})} \\ &\times W_{(E^{v}_{i'},E^{r}_{i'},E^{v}_{n'},E^{r}_{n'}|E_{\text{tot}})}\times W_{(J_{i'},J_{n'},\mu',E_{\text{col}'}|J_{\text{tot}})} \end{aligned} \tag{47}$$

and its probability is

$$P_{(\mathcal{J}',\mathcal{N}'|\mathcal{C})} = \frac{W_{(\mathcal{J}',\mathcal{N}'|\mathcal{C})}}{\Sigma_{\mathcal{J}',\mathcal{N}'} W_{(\mathcal{J}',\mathcal{N}'|\mathcal{C})}}. \quad (48)$$

D. State-to-state cross sections and thermal rate coefficients

The state-to-state cross sections for a given collision energy E_{col} are obtained by distributing the Langevin cross section [Eq. (21)] among the product channels according to

$$\sigma_{\mathcal{J}\mathcal{N}\to\mathcal{J}',\mathcal{N}'}(E_{\mathrm{col}}) = \sigma_c(E_{\mathrm{col}}) \times P_{(\mathcal{J}',\mathcal{N}'|\mathcal{J},\mathcal{N},E_{\mathrm{col}})}, \quad (49)$$

where the state-to-state reaction probabilities are obtained from the reactants-to-complex and complex-to-products state-detailed probabilities summed over all intermediate complex channels:

$$P_{(\mathcal{J}',\mathcal{N}'|\mathcal{J},\mathcal{N},E_{\mathrm{col}})} = \sum_{\mathcal{C}} P_{(\mathcal{J}',\mathcal{N}'|\mathcal{C})} \times P_{(\mathcal{C}|\mathcal{J},\mathcal{N},E_{\mathrm{col}})}. \quad (50)$$

Equations (34) and (48) show that the normalization $\Sigma_{\mathcal{J}'\mathcal{N}'} P_{(\mathcal{J}',\mathcal{N}'|\mathcal{J},\mathcal{N},E_{\mathrm{col}})} = 1$ is automatically fulfilled.

In thermal environments, the motions of the reactants, $\mathcal{J}$ and $\mathcal{N}$, in the laboratory frame exhibit Maxwell–Boltzmann velocity and energy distributions. Based on the properties of the Gaussian distributions representing the reactants in the laboratory frame, the distributions of the relative velocity v_{col} and energy E_{col} in the center-of-mass frame are also Maxwell–Boltzmann with the reduced mass μ,

$$P_{(v_{\mathrm{col}}|T)} = 4\pi \left(\frac{\mu}{2\pi kT}\right)^{3/2} v_{\mathrm{col}}^2 e^{-\mu v_{\mathrm{col}}^2/2kT}, \quad (51)$$

$$P_{(E_{\mathrm{col}}|T)} = 4\pi \left(\frac{\mu}{2\pi kT}\right)^{3/2} \frac{2E_{\mathrm{col}}}{\mu} e^{-E_{\mathrm{col}}/kT}. \quad (52)$$

The reaction probabilities have been calculated in the center-of-mass frame. The state-to-state thermal rate coefficients are obtained from the definition $k = \int v_{\mathrm{col}} \cdot \sigma(v_{\mathrm{col}}) \cdot P(v_{\mathrm{col}}) \cdot dv_{\mathrm{col}}$ and in the energy domain using the substitutions $v_{\mathrm{col}} = \sqrt{2E_{\mathrm{col}}/\mu}$ and $dv_{\mathrm{col}}/dE_{\mathrm{col}} = (2\mu E_{\mathrm{col}})^{-1/2}$. As a result the thermal state-to-state rate coefficients, $k_{\mathcal{J}\mathcal{N}\to\mathcal{J}'\mathcal{N}'}(T)$, are given by

$$\begin{aligned}
k_{\mathcal{J}\mathcal{N}\to\mathcal{J}'\mathcal{N}'}(T) &= \int_{v_{\mathrm{col}}=0}^{\infty} v_{\mathrm{col}} \times \sigma_{\mathcal{J}\mathcal{N}\to\mathcal{J}'\mathcal{N}'}(v_{\mathrm{col}}) \times P_{(v_{\mathrm{col}}|T)} \times dv_{\mathrm{col}} \\
&= \int_{E_{\mathrm{col}}=0}^{\infty} \sqrt{\frac{2E_{\mathrm{col}}}{\mu}} \times \sigma_c(E_{\mathrm{col}}) \times P_{(\mathcal{J}',\mathcal{N}'|\mathcal{J},\mathcal{N},E_{\mathrm{col}})} \times P_{(E_{\mathrm{col}}|T)} \times \frac{dv_{\mathrm{col}}}{dE_{\mathrm{col}}} \times dE_{\mathrm{col}} \\
&= \int_{E_{\mathrm{col}}=0}^{\infty} \sqrt{\frac{2E_{\mathrm{col}}}{\mu}} \times \pi \sqrt{\frac{\alpha q^2}{2\pi\epsilon_0 E_{\mathrm{col}}}} \times P_{(\mathcal{J}',\mathcal{N}'|\mathcal{J},\mathcal{N},E_{\mathrm{col}})} \times 4\pi \left(\frac{\mu}{2\pi kT}\right)^{3/2} \frac{2E_{\mathrm{col}}}{\mu} e^{-E_{\mathrm{col}}/kT} \times \frac{1}{\sqrt{2\mu E_{\mathrm{col}}}} \times dE_{\mathrm{col}} \\
&= k_L \times \int_{E_{\mathrm{col}}=0}^{\infty} P_{(\mathcal{J}',\mathcal{N}'|\mathcal{J},\mathcal{N},E_{\mathrm{col}})} \times \frac{2}{\sqrt{\pi (kT)^3}} \sqrt{E_{\mathrm{col}}} e^{-E_{\mathrm{col}}/kT} dE_{\mathrm{col}},
\end{aligned}$$

with the Langevin rate coefficient being

$$k_L = \sqrt{\frac{\pi\alpha q^2}{\mu\epsilon_0}}. \quad (53)$$

The state-to-state thermal rate coefficients are properly normalized since they verify

$$k_{\mathcal{J}\mathcal{N}}(T) = \sum_{\mathcal{J}'\mathcal{N}'} k_{\mathcal{J}\mathcal{N}\to\mathcal{J}'\mathcal{N}'}(T) = k_L. \quad (54)$$

Based on the above described procedure, state-to-state rate coefficients have been calculated for simulating low-temperature laboratory experiments as discussed below and for simulating H_3^+ and its isotopologues in interstellar environments.[38] As pointed out above in Sec. II C 1, the possible reaction mechanisms as well as the proper implementation of the ergodic principle will influence the results. Therefore a set of different approaches is discussed prior to applications of the microcanonical rate coefficients.

E. Ergodic principle and reaction mechanisms

PST is based on the equiprobability principle; it is a simple thus convenient theory to describe systems but it is only a good approximation in the ergodic limit which considers the microcanonical population as fully relaxed to an equilibrium state in the complexes' PES. As a consequence, a complex channel forgets its history and the decay probabilities are independent of the reactants' channels. Such collision process can therefore be described microscopically as a memoryless Markov chain $(\mathcal{J}\mathcal{N}\mathcal{M}) \to \mathcal{C} \to (\mathcal{J}'\mathcal{N}'\mathcal{M}')$ and be decomposed in the complex formation and complex decay as done here. In this statistical approach, a weight has to be assigned to each isotopic channel. If nothing is known on the number of possible pathways to link a reactant channel with a product channel, a statistical weight of 1 may be associated to an accessible isotopic channel while a weight of 0 is associated to an inaccessible isotopic channel. This implementation of the ergodic principle is called the *weak* ergodic limit. In the *strong* ergodic limit, the statistical weight of an

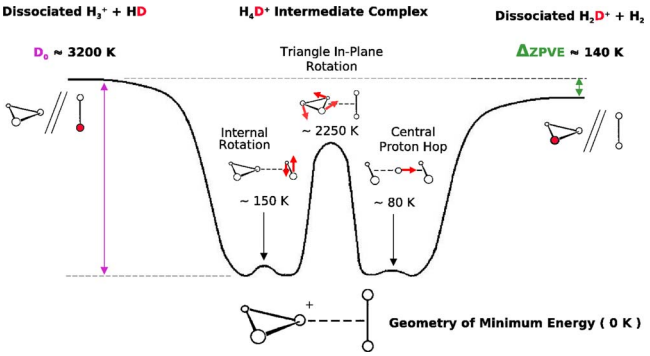

FIG. 2. (Color online) Schematic of the H_4D^+ PES according to calculations on H_5^+ (Refs. 19–21). The minimum energy configuration consist of a H_3^+ triangle entity and a H_2 entity, the charge being localized on the central nucleus. Saddle points for three internal motions are represented as well as the asymptotes for the two isotopic channels. They differ in energy because of zero-point rotational and vibrational energies.

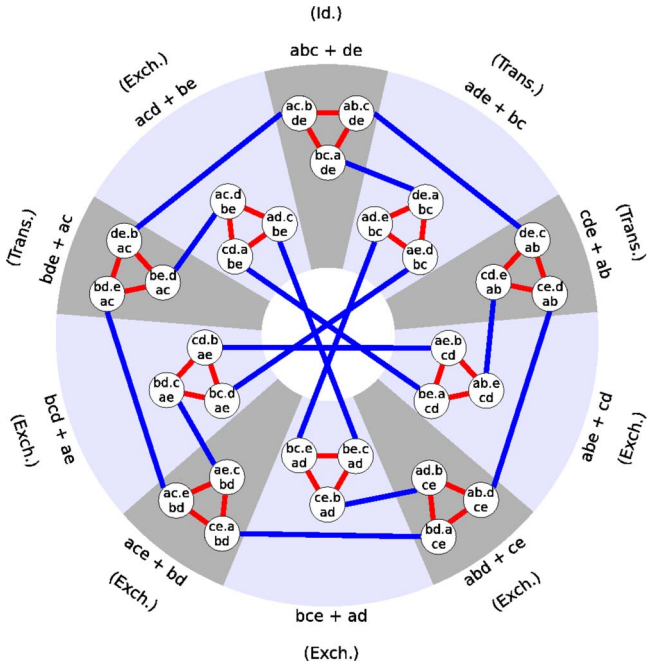

FIG. 3. (Color online) Map of minimum energy arrangements of a H_5^+ isotopic complex. A quartet of arrangements is labeled as ab.c/de with a and b the two outer nuclei of the H_3 moiety, c the central nucleus belonging to the H_3 moiety, and d and e the two nuclei of the H_2 moiety. The 30 quartets of arrangements are interconnected by the H_3 moieties' in-plane rotation (lines within each shade) and the central nucleus hop (lines between shades) internal motions. Each of the ten dissociative asymptotes (shades) is connected to three quartets of arrangements. The one identity, three transfer and six exchange reaction mechanisms are attributed to the dissociative asymptotes assuming (abc+de) is the entrance channel.

isotopic channel is given by its number of accessible dissociative asymptotes, i.e., the degeneracy of reaction mechanisms leading to this isotopic channel. The statistical weights introduced in Sec. II C 1, and consequently the microcanonical rate coefficients derived above for the H_5^+ isotopic system will thus depend on (i) the weak or strong ergodic limit considered as well as on (ii) the feasible reaction mechanisms constrained by the PES.

The H_5^+ considered here is a peculiar system because on the sole consideration of its PES, any entrance channel can potentially access all 5!/3!2!=10 dissociative asymptotes. Its configuration of minimum energy on the PES consists of a H_3 and a H_2 moiety with the charge localized on the central nucleus (see Fig. 2). The two relevant internal motions for nuclear rearrangement are the central nucleus hop with an extremely shallow barrier and the in-plane rotation of the H_3 moiety with a more consequent yet submerged saddle point. Upon the internal rotation, also shown in Fig. 2, the positions of the two outer nuclei of the H_3 moiety or those of the H_2 moiety are rearranged. This internal motion cannot promote any modification of the H_3 and H_2 moieties; therefore it can be ignored in the current treatment and the 5!=120 different minimum energy arrangements are grouped by 2!2!=4 into 30 quartets. As depicted in Fig. 3, the 30 quartets of arrangements are connected to the ten dissociative asymptotes and interconnected by the two relevant internal motions, forming a map in which the microcanonical population can evolve. We discuss two limiting cases to which we refer as (i) *full-scrambling* and (ii) *hop*, neglecting possible centrifugal distortion of the PES and the fact that isotopic substitution in H_5^+ breaks the symmetry of the PES,[21] potentially favoring some particular arrangements.

(i) If both internal motions (hop and in-plane rotation) can proceed efficiently with respect to the dissociation events, the microcanonical population will visit all 120 minimum energy arrangements of the PES corresponding to the full-scrambling limit. Consequently, the complex can probe equally all ten dissociative asymptotes, depicted in Fig. 3. These asymptotes are denoted as one *identity*, three *transfer*, and six *exchange* reaction mechanisms when entering as reactants (abc+de) at the top of Fig. 3.

(ii) If the in-plane rotation of the H_3 moiety is dynamically hindered and only the central nucleus hop can proceed efficiently during the complex lifetime, the central nucleus is locked and the microcanonical population will be equally distributed in two local wells of the PES corresponding to the entrance arrangement (abc+de) and its arrangement connected by the central nucleus hop. In this hop limit, the complex can probe only two dissociative asymptotes corresponding to one identity and one transfer but no exchange reaction mechanism.

As an example, the microcanonical isotopic statistical weights introduced in Sec. II C 1 are given in Table V for the H_2D^++HD collision for the two limiting cases of full scrambling and hop. In case of full scrambling, i.e., the product channel H_3^++D_2 is accessible via one exchange reaction, the H_2D^++HD channel occurs on six accessible asymptotes, and the D_2H^++H_2 channel has three possibilities. Correspondingly, the statistical weights in the strong ergodic limit are 1:6:3 (see right side of table) and in the weak ergodic limit they are 1:1:1. In the following sections, the strong ergodic limit is considered if not stated otherwise. Comparison of the full scrambling and the hop limits to experimental data will give some first semiquantitative insight into the role of dynamical restrictions and reaction mechanisms.

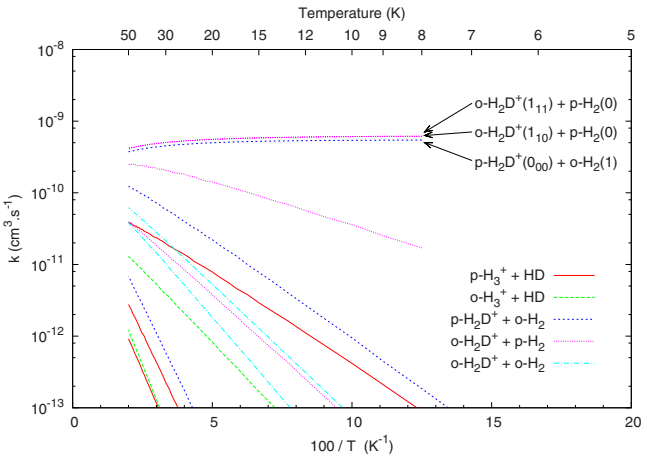

FIG. 4. (Color online) Main state-to-state thermal rate coefficients for the p-$H_2D^+(J_{K_aK_c}=0_{00})$+o-$H_2(J=1)$ collisions. The product channels are represented with different lines according to their isotopic-nuclear spin modifications. Rates for endoergic channels show an Arrhenius behavior while those for exoergic channels are quasitemperature independent.

III. RESULTS

A. Thermal rate coefficients

The outcome of the calculation is a set of several thousands of state-to-state thermal rate coefficients, at present in the temperature range 5–50 K. An example is given in Fig. 4 illustrating an Arrhenius plot of the main state-to-state rate coefficients for p-$H_2D^+(J_{K_aK_c}=0_{00})$+o-$H_2(J=1)$ collisions. Elastic, inelastic, as well as reactive collisions are accounted for. Collisions accessing endoergic states show an Arrhenius behavior with an activation energy very close to the endoergidicity while reactions to exoergic states are quasitemperature independent. Based on the observed temperature dependence it is well justified to parametrize the rate coefficient as $k=\alpha\cdot e^{-\beta/T}$. Such temperature behaviors are also found for the inelastic state-to-state rate coefficients for the *para* and *ortho* ground transitions of H_2D^+ and D_2H^+ in collsions with *para*- and *ortho*-H_2 given in Table VI. These rate coefficients are of particular interest for the modeling of astronomical observations.

We note that our results agree with the ground state-to-nuclear spin species thermal rate coefficients of the $H_3^+ + H_2$ system at 10 K calculated by Park and Light[25] within 3% of their given accuracy. These rates are defined according to

$$k_{\mathcal{JN}\to\Gamma_{i'}\Gamma_{n'}}(T)=\sum_{\mathcal{J}'\in\Gamma_{i'}}\sum_{\mathcal{N}'\in\Gamma_{n'}}k_{\mathcal{JN}\to\mathcal{J}'\mathcal{N}'}(T). \quad (55)$$

Regarding the greater details they accounted for, we conclude that in this temperature range, spectroscopic accuracy of the energy levels, charge-dipole and charge-quadrupole interactions,[46] tunneling, and above-barrier reflections as well as parity conservation do not affect the rate coefficients significantly and can thus be safely neglected.

TABLE VI. Inelastic state-to-state rate coefficients for the *ortho* and *para* ground transitions of H_2D^+ and D_2H^+ in collisions with *para*- and *ortho*-H_2 according to strong ergodicity. The rates are given in the form $k=\alpha e^{-\beta/T}$. The α ($cm^3\,s^{-1}$) and β (kelvin) coefficients were fitted in the temperature range 5–15 K. The Einstein coefficients for spontaneous emission A_{ul} (s^{-1}) (Ref. 34) and the critical densities $n_c=A_{ul}/k_{ul}$ (cm^{-3}) of the transitions for p-H_2 dominated environments are also given.

Reactants		Products			Rate coefficient	
ion	H_2	ion	H_2	ΔE[a]	α[b]	β
p-H_2D^+ ($0_{00}\leftrightarrow 1_{01}$) at 1.370 THz						
p-0_{00}	p-0	p-1_{01}	p-0	−66	1.48(−9)	65.24
p-0_{00}	o-1	p-1_{01}	o-1	−66	5.35(−10)	63.43
p-1_{01}	p-0	p-0_{00}	p-0	+66	4.91(−10)	−0.24
p-1_{01}	o-1	p-0_{00}	o-1	+66	1.96(−10)	−0.93
$A=4.0397\times10^{-3}$				$n_c\approx 8\times10^6$		
o-H_2D^+ ($1_{11}\leftrightarrow 1_{10}$) at 372 GHz						
o-1_{11}	p-0	o-1_{10}	p-0	−18	9.41(−10)	17.88
			o-1	−188	3.20(−10)	186.80
o-1_{11}	o-1	o-1_{10}	p-0	+152	4.36(−11)	−0.56
			o-1	−18	6.47(−10)	17.66
o-1_{10}	p-0	o-1_{11}	p-0	+18	9.36(−10)	−0.17
			o-1	−152	3.69(−10)	150.74
o-1_{10}	o-1	o-1_{11}	p-0	+188	3.71(−11)	−0.03
			o-1	+18	6.43(−10)	−0.21
$A=1.2186\times10^{-4}$				$n_c\approx 1.3\times10^5$		
p-D_2H^+ ($1_{01}\leftrightarrow 1_{10}$) at 692 GHz						
p-1_{01}	p-0	p-1_{10}	p-0	−33	9.13(−10)	33.07
			o-1	−203	2.89(−10)	198.35
p-1_{01}	o-1	p-1_{10}	p-0	+137	6.89(−11)	−1.43
			o-1	−33	6.35(−10)	31.69
p-1_{10}	p-0	p-1_{01}	p-0	+33	9.07(−10)	−0.14
			o-1	−137	5.72(−10)	133.26
p-1_{10}	o-1	p-1_{01}	p-0	+203	4.05(−11)	−0.81
			o-1	+33	6.70(−10)	−0.84
$A=5.0911\times10^{-4}$				$n_c\approx 5.6\times10^5$		
o-D_2H^+ ($0_{00}\leftrightarrow 1_{11}$) at 1.476 THz						
o-0_{00}	p-0	o-1_{11}	p-0	−71	1.32(−9)	69.44
			o-1	−241	3.25(−10)	232.39
o-0_{00}	o-1	o-1_{11}	p-0	+99	1.21(−10)	−1.25
			o-1	−71	9.51(−10)	68.06
o-1_{11}	p-0	o-0_{00}	p-0	+71	4.72(−10)	−0.24
			o-1	−99	3.84(−10)	98.17
o-1_{11}	o-1	o-0_{00}	p-0	+241	1.78(−11)	−1.04
			o-1	+71	3.66(−10)	−0.73
$A=3.3031\times10^{-3}$				$n_c\approx 7\times10^6$		

[a]Internal energy difference in Kelvin.
[b]The format $a(-b)$ represents $a\times10^{-b}$.

B. Microcanonical and canonical approaches

In order to test the microcanonical model, we compared the calculated set of state-to-state thermal rate coefficients to thermodynamical equations by the intermediate of a state-detailed master equation.

1. State-detailed master equation

Consider an ensemble of H_3^+ isotopologues in a given H_2 isotopic environment with respective state populations $[\mathcal{J}]$

and $[\mathcal{N}]$ in cm^{-3}. The fluxes of populations can be described by a set of differential equations corresponding to a state-detailed chemical master equation. Within the dilute limit, i.e., the assumption that the ions are much less abundant than the neutrals ($\Sigma_{\mathcal{J}}[\mathcal{J}] \ll \Sigma_{\mathcal{N}}[\mathcal{N}]$), the populations of the H_3^+ isotopologues evolve on a much shorter time scale than the neutral environment's populations; hence the populations of the neutrals are almost unaffected by the ionic ensemble. Consequently, the master equation can be decomposed in (i) an ionic part assuming a static environment and (ii) a neutral part considering the ionic ensemble in pseudoequilibrium with the environment itself.

The master equation describing the fluxes of populations of the ionic ensemble is defined by

$$\frac{d[\mathcal{J}]}{dt} = \sum_{\mathcal{J}'} [\mathcal{J}']R_{\mathcal{J}'\to\mathcal{J}} - [\mathcal{J}]\sum_{\mathcal{J}'} R_{\mathcal{J}\to\mathcal{J}'}, \tag{56}$$

the first and second terms respectively representing the inflow and outflows of the ion state $\mathcal{J}$ from/to the other ion states $\mathcal{J}'$. The elements $R_{\mathcal{J}\to\mathcal{J}'}$ are conversion rates in s^{-1} defined as

$$R_{\mathcal{J}\to\mathcal{J}'} = \sum_{\mathcal{N}}\sum_{\mathcal{N}'} [\mathcal{N}]k_{\mathcal{J}\mathcal{N}\to\mathcal{J}'\mathcal{N}'}(T), \tag{57}$$

with $[\mathcal{N}]$ the neutral states' populations here considered as constant. They correspond to given isotopic enrichments $[HD]/[H_2]$ and $[D_2]/[H_2]$, o/p ratios of H_2 and D_2, and a rotational temperature T_{rot}. Only bimolecular processes with $\mathcal{N}$ as a collision partner are considered. The state-to-state thermal rate coefficients are those corresponding to the kinetic temperature of the neutral environment T_{kin}. Contrarily to the nuclear spins (o/p ratios), the rotational and kinetic degrees of freedom are often very well thermalized; therefore we considered a single temperature T.

The steady-state populations $[\mathcal{J}]_{ss}$ of the H_3^+ isotopologues which are solution to the set of equations $d[\mathcal{J}]/dt = 0$ can be easily obtained through diagonalization of the $\mathbf{R}_{\mathcal{J}}$ matrix consisting of the $\mathbf{R}_{\mathcal{J}\to\mathcal{J}'}$ elements. Furthermore, the master equation describing the population fluxes of the neutral environment is defined by

$$\frac{d[\mathcal{N}]}{dt} = \sum_{\mathcal{N}'} [\mathcal{N}']R_{\mathcal{N}'\to\mathcal{N}} - [\mathcal{N}]\sum_{\mathcal{N}'} R_{\mathcal{N}\to\mathcal{N}'}, \tag{58}$$

with the conversion rates $R_{\mathcal{N}\to\mathcal{N}'}$ of the $\mathbf{R}_{\mathcal{N}}$ matrix defined as

$$R_{\mathcal{N}\to\mathcal{N}'} = \sum_{\mathcal{J}}\sum_{\mathcal{J}'} [\mathcal{J}]_{ss}k_{\mathcal{J}\mathcal{N}\to\mathcal{J}'\mathcal{N}'}(T). \tag{59}$$

2. Thermal equilibrium

Consider the following exothermic reaction with forward and backward rate coefficients k_f and k_b,

$$A + B \underset{k_b}{\overset{k_f}{\rightleftharpoons}} C + D + \Delta E_0. \tag{60}$$

The canonical equilibrium constant K at a temperature T given by statistical mechanics[30,47,48] is

TABLE VII. Canonical isotopic statistical weight $g:g'$ of the eight isotopic reactions for the full-scrambling (FS) and the hop limits used in Eq. (61). In the weak (W) ergodic limit, only accessibility of an isotopic channel is accounted for. In the strong (S) ergodic limit, the dissociative asymptotes are counted.

				FS		Hop	
Reactants		Products		S	W	S[a]	W
H_2D^+	D_2	D_3^+	H_2	3:1	1:1	3:1	1:1
H_3^+	D_2	D_2H^+	H_2	1:3	1:1	1:3	1:1
D_2H^+	HD	D_3^+	H_2	6:1	1:1	0:0	0:0
H_3^+	HD	H_2D^+	H_2	4:6	1:1	2:3	1:1
H_2D^+	HD	D_2H^+	H_2	6:3	1:1	2:1	1:1
D_2H^+	D_2	D_3^+	HD	6:4	1:1	3:2	1:1
H_3^+	D_2	H_2D^+	HD	1:6	1:1	0:0	0:0
H_2D^+	D_2	D_2H^+	HD	3:6	1:1	1:2	1:1

[a]Averaged values assuming the three nuclei of the H_3^+ isotopologue can equiprobably lock in the center of the complex.

$$K(T) = \frac{k_f}{k_b} = \frac{g'}{g}\left(\frac{\mu'}{\mu}\right)^{3/2}\frac{Q_C Q_D}{Q_A Q_B}\exp\left(\frac{-\Delta E_0}{kT}\right), \tag{61}$$

where μ and μ' are the reduced masses of $A+B$ and $C+D$,respectively, and ΔE_0 is the zero-point energy difference. The terms g and g' were added with respect to prior publications. These canonical isotopic statistical weights correspond to the degeneracies of the backward and forward reaction mechanisms. They are a consequence of the statistical weights used in the microcanonical description. These weights are given in Table VII. It is obvious that, for example, the $g:g'$ ratio of the $H_3^+ + D_2 \rightleftharpoons D_2H^+ + H_2$ reaction is 1:3 in the strong ergodic and full-scrambling limit, because there are three ways to pick a H from three H but only one to form $H_3^+ + D_2$.

The Q in Eq. (61) are the partition functions of the species at the temperature T defined by

$$Q_A(T) = \sum_i N_{A_i}(T), \tag{62}$$

$$N_{A_i}(T) = g_i \exp(-E_i/kT), \tag{63}$$

with N_{A_i} the population of the ith state of species A, g_i its nuclear spin and rotational degeneracy, and E_i its energy. It should be reminded that Eq. (61) describes thermal equilibrium only, when all the species are effectively internally and kinetically Boltzmann distributed. The equilibrium constants of the eight isotopic reactions are plotted in Fig. 5 using the strong ergodicity principle and the full-scrambling hypothesis. It is noteworthy that every equilibrium constant seems to converge to unity at infinite temperature. Moreover, on the whole temperature range 5–300 K, i.e., from the low toward the high-temperature limit,[48] we observe the strict equalities

$$\frac{K_1}{K_2} = \frac{K_3}{K_4} = \frac{K_6}{K_7} \quad \text{and} \quad \frac{K_3}{K_6} = \frac{K_5}{K_8}, \tag{64}$$

with K_i the equilibrium constant of reaction (i) [(i) as in Fig. 5]. Those unexpected relations might be explained by symmetric isotopic substitutions yet they are nonintuitive since they involve vibrational energies, rotational constants, and

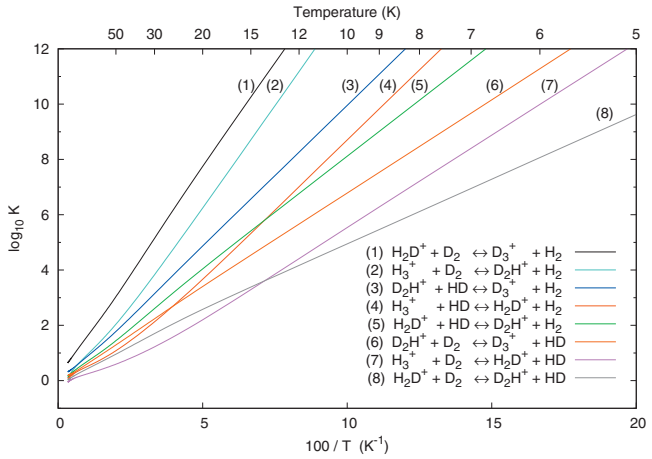

FIG. 5. (Color) Equilibrium constants [Eq. (61)] of the eight isotopic reactions with the full-scrambling limit and the strong ergodicity principle.

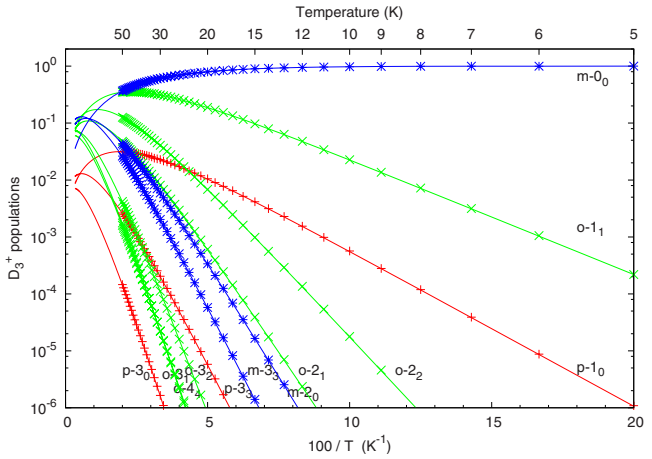

FIG. 6. (Color online) Populations of the 12 lowest rotational levels of D_3^+. Solid lines are thermal populations and crosses are the steady-state populations in a thermal D_2 environment derived from the master equation using the set of state-to-state rate coefficients.

densities of states as well as nuclear spin selection rules and degeneracies.

The canonical equilibrium constant is also related to the chemical equilibrium (steady-state populations or number densities) by

$$K(T) = \frac{[C]_{ss}[D]_{ss}}{[A]_{ss}[B]_{ss}}. \tag{65}$$

The canonical balance corresponding to Eqs. (61) and (65) can be transposed to specific internal states of the species resulting in the detailed balance. Although it also holds for reactive collisions, this principle is mostly known for nonreactive, inelastic collisions, i.e., with $(A,B)=(C,D)$, $\Delta E_0=0$, $\mu=\mu'$, and $g=g'$:

$$A_i + B_j \underset{k_b}{\overset{k_f}{\rightleftharpoons}} A_{i'} + B_{j'}, \tag{66}$$

$$K(T) = \frac{k_f}{k_b} = \frac{N_{A_i} N_{B_j}}{N_{A_{i'}} N_{B_{j'}}} \tag{67}$$

$$= \frac{[A_{i'}]_{ss}[B_{j'}]_{ss}}{[A_i]_{ss}[B_j]_{ss}}. \tag{68}$$

3. Comparison and analysis

Steady-state populations of the H_3^+ isotopologues were obtained by solving the master equation for various thermal and nonthermal neutral environments [Eqs. (56) and (57)]. These populations are compared to thermal populations derived according to the canonical balance [Eqs. (61) and (65)] and the detailed balance [Eqs. (67) and (68)]. We present here a sample of results.

The purely hydrogenated and deuterated systems were first simulated by employing a pure thermal H_2 or D_2 environment at various temperatures. As shown in Fig. 6 for the purely deuterated system, $D_3^+ + D_2$, the master equation renders thermalized D_3^+ steady-state populations thereby confirming that the set of state-to-state thermal rate coefficients fulfills the isotopically nonreactive detailed balance [Eq. (67)]. Note that an isotopically nonreactive collision can still be reactive in the sense of *homonuclear exchange*.

We also simulated environments at different temperatures with terrestrial and cosmic deuterium abundances, i.e., $HD/H_2 = 3.2\times10^{-4}$ and 3.2×10^{-5}, respectively, neglecting D_2. The o/p ratio of H_2 was set as thermal or fixed between its high-temperature limit of 3 down to 10^{-7}. As an example, the steady-state H_2D^+/H_3^+ isotopic ratio is shown in Fig. 7. The deuterium fractionation in thermal o/p-H_2 environment increases sharply toward low temperatures as suggested by the equilibrium constant of reaction (4) in Fig. 5 which is governed by the endothermicity. For a fixed superthermal o/p ratio of H_2, the H_2D^+/H_3^+ ratio levels off to a maximum value since the quantity of o-H_2 dominates the back reaction with its 170 K internal energy irrespective of the tempature and the endothermicity. The role of o-H_2 and the lowest

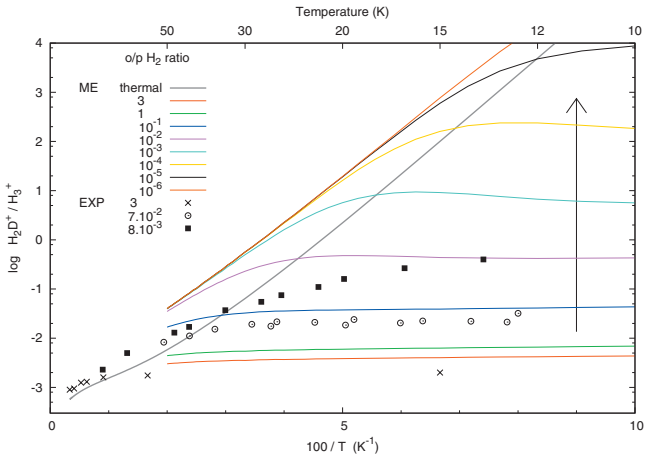

FIG. 7. (Color) Steady-state H_2D^+/H_3^+ isotopic fractionation in a H_2 environment with terrestrial deuterium abundance ($HD/H_2 = 3.2\times10^{-4}$). The solid lines are results of the master equation (ME) using the strong ergodicity principle for various o/p ratios of H_2 (no D_2 is considered). The arrow indicates a decreasing o/p ratio of H_2. The points are experimental results (EXP) for o/p-H_2=3, 7×10^{-2}, and 8×10^{-3} (see Sec. IV C).

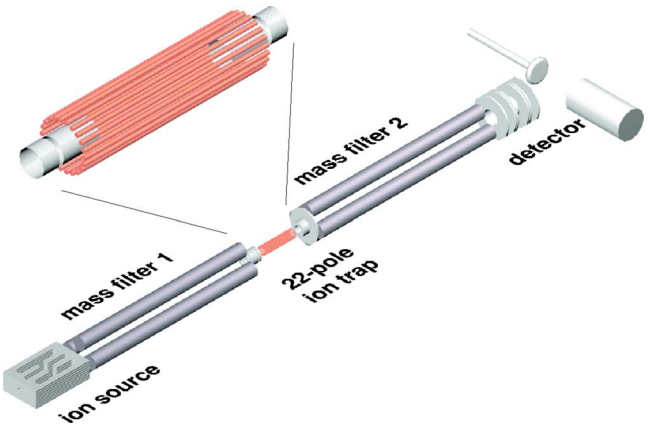

FIG. 8. (Color online) Schematic of the trapping apparatus. The H_3^+ ions are produced in the storage ion source and pulsed through the quadrupole mass filter 1 into the 22-pole ion trap. This trap, consisting of 22 electrodes forming a cylindrical structure, is mounted on a closed cycle helium refrigerator. On entrance, the ions are cooled down to the ambient temperature by a short intense pulse of He atoms. During the storage period of 10–1000 ms, the ions are subject to a constant density of H_2 or HD reactant gas. The result of the interaction is detected by extracting the stored ion cloud through the quadrupole mass filter 2 and counting the number of product ions in the detector.

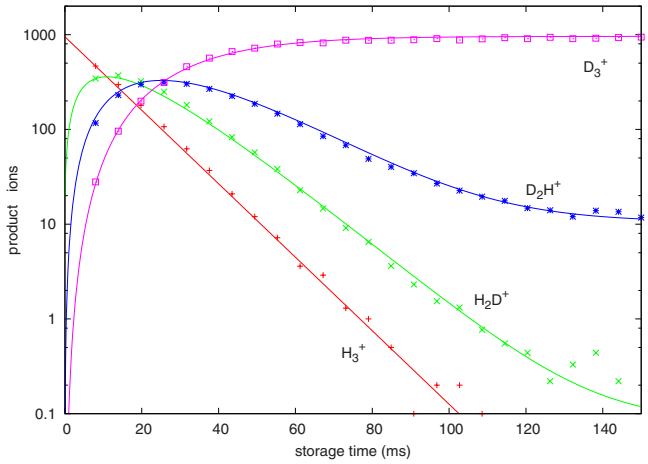

FIG. 9. (Color online) Sequential deuteration of H_3^+ in HD with a number density of 6.3×10^{10} cm^{-3} at a nominal temperature of 13.5 K. Due to the exothermicity of the reaction chain, a constant number density of helium of about 6×10^{12} cm^{-3} has been applied to ensure full thermalization of all reactants. The lines are the solutions of a rate equation system fitted to the experimental data yielding rates of 1.30×10^{-9}, 1.30×10^{-9}, and 1.05×10^{-9} cm^3 s^{-1} for the deuteration of H_3^+, H_2D^+, and D_2H^+, respectively.

o-H_2D^+ rotational states has already been discussed qualitatively by Gerlich *et al.*[18] On the contrary, a subthermal o/p-H_2 ratio leads to a higher H_2D^+/H_3^+ ratio since the back reaction is then governed by p-H_2 and its larger endoergicity. The H_2D^+/H_3^+ as well as the D_2H^+/H_2D^+ and D_3^+/D_2H^+ (the latter two not shown in Fig. 7) steady-state ratios in the thermal o/p-H_2 environment are all consistent with the canonical equilibrium constants of reactions (4), (5), and (3) in Fig. 5, respectively. Moreover, each H_3^+ isotopologue is well thermalized internally.

We thereby show that the calculated state-to-state thermal rate coefficients fulfill the canonical and detailed balance within a few per thousand according to the full-scrambling hypothesis and the strong ergodicity principle. These results, which are observed for the weak and strong ergodic limits, demonstrate that the microcanonical model is consistent with the canonical description. While this result is gratifying, simulating experimental results or astrophysical observations with the state-to-state rate coefficients is posing a more serious test to the microcanonical model.

IV. EXPERIMENTAL SECTION

A. 22-pole ion trap apparatus

To study the $H_3^+ + H_2$ isotopic system, we extended the measurements described by Gerlich *et al.*[18] using the same apparatus depicted in Fig. 8. The core of the setup, the temperature variable 22-pole ion trap, has been described in detail elsewhere.[49,50] It is enclosed in stainless steel walls which are mounted on a closed cycle helium refrigerator. The temperature of these walls, monitored by two silicon diodes, can range from ~300 K down to 13.0 ± 0.5 K.

H_3^+ parent ions are produced in a storage ion source by electron bombardment of n-H_2 and pulsed via a first quadrupole mass filter into the 22-pole ion trap. There, the ion cloud is exposed to a constant density of reactant gas (HD or H_2 with natural traces of HD) thermalized to the surrounding walls. Additionally, pulsed or constant He gas can be admitted to the trap. The gas number densities were accurately determined with a pressure ion gauge calibrated against a spinning rotor gauge prior to the measurements and were kept below 10^{13} cm^{-3} in order to avoid ternary association.[51] After a storage period of 10–1000 ms, the ions are extracted, mass selected in the second quadrupole mass filter, and counted in a Daly-type ion detector.

The storage cycle is repeated for several trapping times counting the H_3^+, H_2D^+, D_2H^+, or D_3^+ products. As illustrated in Fig. 9, we obtain the time evolution and steady-state populations of each isotopologue from which we can fit reaction rate coefficients using a standard system of differential equations.

Prior to its introduction into the trap, the H_2 reactant gas could be flown through a p-H_2 generator in order to catalyze the conversion of *ortho*-H_2 into *para*-H_2. This converter contains a paramagnetic compound (Fe_2O_3 powder) confined in a copper block mounted onto a closed cycle helium refrigerator. The temperature of the catalyst was measured by a silicon diode mounted on the copper block and could be tuned in the range 11–50 K in order to vary the o/p ratio of the outflowing H_2 down to 8×10^{-3}. The o/p ratio was calibrated with an accuracy of 20% in the 22-pole ion trap using the proton abstraction reaction $N^+ + H_2 \rightarrow NH^+ + H$ as described in Ref. 52. We also monitored *in situ* the HD content of natural H_2 using a H_2O^+ beam and the proton (deuteron) abstraction reactions

$$H_2O^+ + H_2 \rightarrow H_3O^+ + H, \tag{69}$$

$$H_2O^+ + HD \rightarrow H_3O^+ + D \quad 0.57 \tag{70}$$

$$\rightarrow H_2DO^+ + H \quad 0.43, \tag{71}$$

with the given branching ratios determined *in situ* using pure HD target gas. In experiments with unprocessed n-H_2, we obtain the product ratio $H_2DO^+/H_3O^+ = 1.1 \times 10^{-4}$. Assuming that both reactions with H_2 and HD proceed with the Langevin rate, that is,

$$\frac{k_{H_2O^+ + HD}}{k_{H_2O^+ + H_2}} = \sqrt{\frac{\mu_{H_2O^+ + H_2}}{\mu_{H_2O^+ + HD}}} = 0.837, \tag{72}$$

we derive a HD fraction of 3.1×10^{-4} which corresponds to the expected terrestrial deuterium hydride abundance. However, when starting the converter, the HD content of the processed H_2 was depleted by about one order of magnitude caused apparently by isotopic preferential freezing on the cold catalyst.[53] After some hours of operation, the terrestrial fraction was approached again. Therefore, to ensure the terrestrial HD fraction in the outflowing p-H_2, the converter was run 1 day prior to the experiments. In summary, great care has been taken to accurately determine the number densities of the neutral reaction partners as has been pointed out by Gerlich *et al.*[32]

B. Deuteration rates with HD

We measured the deuteration rate coefficients of H_3^+, H_2D^+, and D_2H^+ with HD between 13 and 210 K in the presence of helium buffer gas ([He] ≫ [HD]). The target gas HD has been purchased from Cambridge Isotope Laboratories, Inc., which specify the purity of the deuterium hydride to be 97%, the rest mainly being H_2 and D_2. The results are compiled in Fig. 10 together with previously published values. Our results are in good agreement with those of Adams and Smith[29] and Giles *et al.*[30] showing systematic temperature dependencies overlapping in the common temperature range. The low-temperature rate coefficients from Gerlich *et al.*[18] are systematically lower than ours by a factor of ~4. This important difference needs some special attention later.

All the rate coefficients approach the Langevin value at low temperature. At 300 K, (i) the deuteration rate coefficient of H_3^+ is still very fast, (ii) the deuteration rate coefficient of $H_2D^+ + HD$ drops by a factor of 2–3 between 10 and 300 K, and (iii) the deuteration rate coefficient of $D_2H^+ + HD$ drops by one order of magnitude over the same temperature range. Contributions from D_2 contaminations (~1.5%) in HD do not change these findings. These trends are all consistent with the departure from the full-scrambling to the hop limit toward high temperatures. Indeed, in the hop limit when one nucleus of the H_3^+ isotopologue locks in the center of the complex, (i) the deuteration of H_3^+ can still proceed on every collision, (ii) the deuteration of H_2D^+ can only proceed when the deuterium nucleus is locked in the center, i.e., with an upper limit for the rate coefficient of $\sim k_L/3$, and (iii) the deuteration of D_2H^+ would be unfeasible under these circumstances, i.e., the rate coefficient would practically approach zero. However, direct mechanisms without complex formation may have to be considered at higher energies. This interpretation of the current observation is in qualitative agreement with the experimental results from Cordonnier *et al.*[31] on the $H_3^+ + H_2$ system at ~400 K also showing an incomplete scrambling. They derived statistical weights for the transfer:exchange reaction mechanisms of 2.4:1 which are in between the full-scrambling and hop limits with statistical weights for the identity:transfer:exchange reaction mechanisms of 1:3:6 and 1:1:0, respectively.

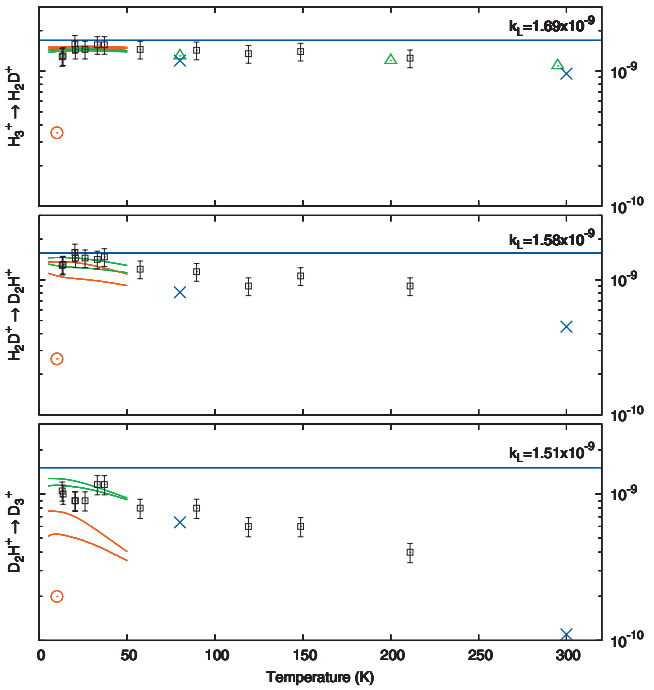

FIG. 10. (Color) Deuteration rate coefficients of H_3^+, H_2D^+, and D_2H^+ with HD. The data points are experimental values corresponding to Gerlich *et al.* (Ref. 18) (circles), Adams and Smith (Ref. 29) (triangles), Giles *et al.* (Ref. 30) (crosses), and this work (squares). The upmost lines show the Langevin limits. The short lines are the species-to-species rate coefficients of the H_3^+ isotopologues' *para* and *ortho* modifications with HD calculated with the full-scrambling hypothesis for the weak (green) and strong (red) ergodicity principles.

The presented experiments yield species-to-species rate coefficients without any information on the internal state distributions of the H_3^+ isotopologues. In order to compare them with theory, we overlaid in Fig. 10 the calculated species-to-species rate coefficients for the H_3^+ isotopologues' *para* and *ortho* nuclear spin modifications, assuming each *para* and *ortho* reactants are internally thermalized by the dominant helium buffer gas. The rates are shown according to the weak and strong ergodic limits. The deuteration rate coefficients of H_3^+ and H_2D^+ are more or less state independent of the nuclear spin modification and they are in very good agreement with the measured rates irrespective of the ergodic limit used. The same observation holds for the deuteration rate coefficients of D_2H^+ based on the weak ergodic limit while those based on the strong ergodic limit are lower, almost by a factor of 2 with a more pronounced drop towards higher temperatures.

C. Steady state in H_2(HD)

Another critical test for any theoretical determination of state-to-state rate coefficients is the steady-state isotopic fractionation of H_3^+. It is also a crucial parameter for the deuterium astrochemistry in cold molecular environments[10,15,38] which can be derived from astronomical observations. As a result, it can be considered a benchmark for comparison between theory, experiment, and observation.

The steady-state H_2D^+/H_3^+ ratio has been measured in H_2 with terrestrial abundance of HD for o/p ratios of 8×10^{-3}, 7×10^{-2}, and 3 with the temperature of the 22-pole ion trap ranging from 13 to 50 K. Results are shown in Fig. 7 together with theoretical values from the master equation based on the strong ergodic limit. Results at the lowest temperatures are in good agreement with Gerlich *et al.*[18] Following their description, our forward rate coefficient being higher by a factor of ~4 together with an even equilibrium constant point at backward rate coefficients also a factor of ~4 higher. Indeed, a value in the range of 2×10^{-10} cm^3 s^{-1} for the backward rate coefficient has also been measured directly by injecting H_2D^+ ions into n-H_2 target gas.

Our theoretical and experimental results shown in Fig. 7 are in reasonable agreement presenting similar trends. However, significant differences are found for the experiment at a H_2 o/p ratio of 0.8×10^{-2} in comparison to the theoretical curve for 10^{-2}. The discrepancy is likely due to an improper thermalization of the ions to the trap's walls. Previous detailed spectroscopic studies of H_2D^+ and D_2H^+ ions showed an ion kinetic temperature of 27 K when the nominal temperature of the trap's walls was 17 K. Reasons for this discrepancy are discussed in Refs. 54–56 and improvements to the ion thermalization at the lowest wall temperatures are currently explored. Despite these difficulties, the general trend of the H_2D^+/H_3^+ ratio as a function of temperature and o/p ratio of H_2 agree very well but follow up experiments at fully thermalized conditions will pose a more quantitative test for the current and future theoretical work.

The agreement with the experimental H_2D^+/H_3^+ ratio is better for the predictions based on the weak ergodic limit (not shown in Fig. 7) as compared to the strong ergodic limit results presented in Fig. 7. The former values are lower by a factor of ~6/4 as can be inferred from Table VII.

V. DISCUSSION

Despite the subtle discrepancies between experiment and theory the general trends are well reproduced. Therefore this work clearly demonstrates the utility of the microcanonical model. In fact the agreement between the two supports the assumption of full scrambling in H_5^+ at low temperatures with an increasing influence of dynamical restrictions perhaps to the limit of a nonergodic behavior at higher energies and temperatures. In any case, the rate coefficients of this study might serve as a test to compare any new experiment, astrophysical modeling, or a more realistic theoretical approach such as scattering calculations which should be feasible for this five, light nuclei system even at a full quantum level when comparing to similar systems of current research.[57] Regardless of these future developments some other aspects deserve attention.

Regarding the complexity of state-detailed chemical models, a reduced model neglecting the rotational states and considering only the nuclear spin modification of the isotopologues may be preferred.[10,15,38] For this purpose, one can use (i) ground state-to-species rate coefficients [see Eq. (55) and the Appendix] on the basis that for low temperatures or for low H_2 densities, only the ground state of each isotope-nuclear spin species is significantly populated or (ii) thermal species-to-species (i.e., canonical) rate coefficients by considering each isotope-nuclear spin species as internally thermalized. Such reduced models can account for the efficient pumping from p-H_2D^+ to H_3^+ via o-H_2D^+ in collisions with the energetic o-H_2 as well as nonthermal *ortho*-(*meta*)-*para* ratios. However, it cannot account for collisional pumping within the rotational ladder of each isotope-nuclear spin species as it cannot account for radiative cooling. This limitation may result in the overestimation or underestimation of the isotopic fractionation of H_3^+ in astrochemical modeling.

A principal limitation to the use of the microcanonical approach appears for nonthermal environments. State-to-state or species-to-species *thermal* rate coefficients are based on the fact that all internal states are kinetically thermalized. Using thermal rate coefficients in a time dependent or steady-state model thus implies that the kinetic degrees of freedom of all internal states are thermalized at all times. However, this assumption can be wrong in environments far from thermal equilibrium since the exchange of energy between the different degrees of freedom can lead to kinetic heating (or cooling). As an example, in an environment very far from equilibrium such as H_2 at $T_{kin}=T_{rot}=10$ K with o/p=3, the H_3^+ ions would be frequently colliding with o-H_2. Since the rotational and kinetic degrees of freedom completely mix their energies during the collision process and that o-H_2 can relax to p-H_2 by exchanging a proton, the H_3^+ ions would keep absorbing a significant fraction of the 170 K internal energy of o-H_2, thereby exciting their rotational and kinetic degrees of freedom to mean energies much higher than the initial 10 K. The H_3^+ ions would be kinetically heated. Thermal rate coefficients are thus incorrect for such environments.

The master equation based on thermal state-to-state rate coefficients presented in Sec. III B 1 works on the internal phase space only and implicitly forces the kinetic degree of freedom to be thermally distributed. Therefore, it cannot account for kinetic heating just as it violates the first law of thermodynamics in nonthermal environments. The steady-state and time-dependent populations which follow from it are therefore biased. In order to mend this statistical mechanical problem, a stochastic method working in the full phase space was proposed[37] but it has not yet been applied to the $H_3^+ + H_2$ system. Note that this kinetic heating effect applies to all species which can exchange a proton with H_2, thus also to CH_3^+, $C_2H_2^+$, and their isotopologues and particularly the light H^+.

VI. CONCLUSIONS

A microcanonical model used to calculate thermal state-to-state rate coefficients for all $H_3^+ + H_2$ isotopic variants in the temperature range 5–50 K has been derived. Full scrambling of the nuclei during the intermediate complex lifetime was assumed. In addition, both weak and strong ergodic limits, respectively neglecting and accounting for the degeneracies of the reaction mechanisms, were tested. In both cases, the resulting set of rate coefficients was successfully compared to the corresponding canonical approach by the intermediate of a state-detailed master equation. Such microcanonical model can be straightforwardly applied to other scrambling isotopic systems such as $CH_3^+ + H_2$.

Extended measurements with a 22-pole ion trap were performed studying, in particular, the deuteration chain of H_3^+ with HD at low temperatures. In general, agreement between experiment and microcanoncical model was found. The temperature dependence of the experiment also agrees with previous experiments at higher temperatures.[29,30] However, the deuteration rate coefficient at the lowest temperature is faster than previously reported by Gerlich *et al.*[18] This is a very surprising result as the measurements have been conducted in the same setup but with a different trap. Recent spectroscopic investigations show that the ion temperature is of concern. However, similar steady-state H_2D^+ to H_3^+ ratios in the different experiments hint at similar trap temperatures. Still, it is quite possible that lower temperatures were reached in the previous study. However, it is questionable whether the rate coefficient will show a drastic drop over a temperature range of 5–10 K. Therefore more systematic studies under conditions of proper thermalization are needed. Technical improvements of the current trap setup are underway.

The agreement between our experimental and theoretical results supports the full-scrambling hypothesis assumed for the calculations. In particular, the relatively fast $D_2H^+ + HD \rightarrow D_3^+ + H_2$ reaction at low temperatures is a clear evidence for efficient exchange reaction mechanisms. Toward higher temperatures, experimental results suggest partial scrambling in favor of the transfer reaction mechanism. State specific experimental rate coefficients which could be obtained with spectroscopic tools[54,55] would serve as a more stringent test for theory.

State-to-state and state-to-nuclear spin species rate coefficients based on the weak and strong ergodic limits as well as equilibrium constants and partition functions are available online as supplementary material.[58] Regarding the underlying physical interpretation, we recommend to use the rate coefficients based on the strong rather than the weak ergodicity principle although our current experimental results tend to partially support the latter.

State-detailed astrochemical models of the H_3^+ isotopologues are now accessible despite their greater complexity. With the advent of a new generation of telescopes and observation facilities (see Ref. 59, Table III), the detection limits and spatial resolutions of $o\text{-}H_2D^+$ and $p\text{-}D_2H^+$ ground state transitions will be significantly improved and those of $p\text{-}H_2D^+$ and $o\text{-}D_2H^+$ will become accessible. Since their critical number densities (see Table VI) are in the typical range of prestellar cores and protostellar objects, coupling between radiative and collisional processes ought to be considered for a good interpretation of the astronomical observations and exact chemical modeling.

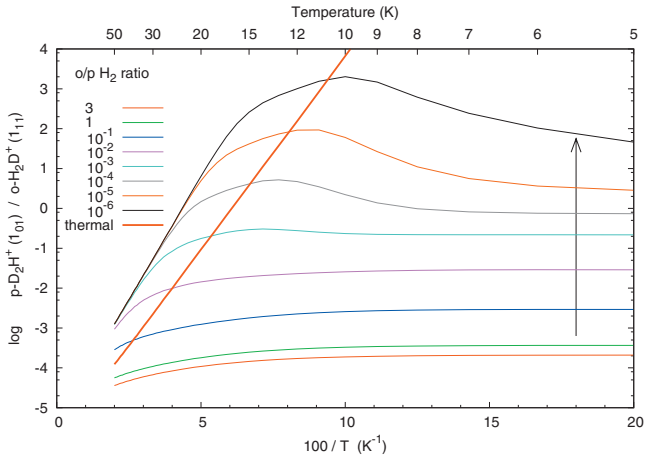

FIG. 11. (Color) The $p\text{-}D_2H^+(1_{01})/o\text{-}H_2D^+(1_{11})$ steady-state ratio as a function of temperature for pure molecular hydrogen environments with deuterium cosmic abundance ($HD/H_2 = 3.2 \times 10^{-5}$) and various $o/p\text{-}H_2$ ratios. The arrow indicates a decreasing o/p ratio of H_2. Radiative processes are not considered here.

The H_3^+ isotopologues are greatly entangled with their H_2 environment, namely, the HD/H_2 ratio, the temperature, and the influential H_2 *ortho*-to-*para* ratio. The latter can be a serious limiting factor for the H_3^+ deuterium fractionation which is a cornerstone of the coolest astrochemistry. The H_2 o/p ratio thus has to be considered in models of cold environments (~10 K) where extreme molecular deuteration can occur. For the same reason, the H_3^+ isotopologues are likely the ideal tracers for the H_2 o/p ratio as illustrated in Fig. 11. We hope that the new tools developed here will shed light on the nonthermal o/p ratio of H_2 and its relaxation during stellar formation.[16,17,38]

ACKNOWLEDGMENTS

This work has been supported by the FP 6 European network "QUASAAR" and the Deutsche Forschungsgemeinschaft (DFG) via FOR 388 "Laboratory Astrophysics" and SFB 494.

APPENDIX: GROUND STATE-TO-SPECIES RATE COEFFICIENTS

Table VIII contains ground state-to-species rate coefficients with nuclear spin modification details.

TABLE VIII. Ground state-to-species rate coefficients with nuclear spin modification details [see Eq. (55)] according to the full-scrambling hypothesis and the strong ergodicity principle. The rows are the ground state reactants and the columns are the product species. The rates are given in the form $k=\alpha e^{-\beta/T}$. The α ($cm^3\ s^{-1}$) and β (kelvin) coefficients were fitted in the temperature range 5–20 K if the rates were higher than $10^{-17}\ cm^3\ s^{-1}$, else up to 50 K. The α coefficients are given with the format $a(-b)$ representing $a\times10^{-b}$. The F refer to reactions strictly forbidden by nuclear spins.

5 H system

		$p\text{-}H_3^+$ $p\text{-}H_2$	$p\text{-}H_3^+$ $o\text{-}H_2$	$o\text{-}H_3^+$ $p\text{-}H_2$	$o\text{-}H_3^+$ $o\text{-}H_2$
$p\text{-}H_3^+$	$p\text{-}H_2$	1.89(−9) 0.00	8.16(−10) 164.9	F	5.88(−10) 198.2
$p\text{-}H_3^+$	$o\text{-}H_2$	2.98(−10) −0.69	1.13(−9) −0.19	3.46(−10) −0.69	8.03(−10) 32.6
$o\text{-}H_3^+$	$p\text{-}H_2$	F	1.50(−9) 136.2	1.84(−9) −0.26	8.84(−9) 170.0
$o\text{-}H_3^+$	$o\text{-}H_2$	1.04(−10) 0.00	4.00(−10) −0.19	9.67(−11) −0.14	1.29(−9) 0.07

4 H-1 D system

		$p\text{-}H_3^+$ HD	$o\text{-}H_3^+$ HD	$p\text{-}H_2D^+$ $p\text{-}H_2$	$p\text{-}H_2D^+$ $o\text{-}H_2$	$o\text{-}H_2D^+$ $p\text{-}H_2$	$o\text{-}H_2D^+$ $o\text{-}H_2$
$p\text{-}H_3^+$	HD	1.55(−10) −1.05	5.71(−11) 32.25	3.11(−10) −0.71	4.93(−10) 0.95	6.08(−10) −1.08	5.71(−10) 25.8
$o\text{-}H_3^+$	HD	2.87(−11) −0.38	1.62(−10) −0.94	F	1.70(−10) −0.44	2.22(−10) −0.47	1.11(−9) 0.35
$p\text{-}H_2D^+$	$p\text{-}H_2$	2.46(−10) 226.5	F	1.79(−9) −0.01	F	F	1.02(−9) 256.1
$p\text{-}H_2D^+$	$o\text{-}H_2$	1.48(−10) 58.8	9.32(−9) 94.6	F	5.29(−10) −0.18	1.26(−9) 0.06	6.04(−10) 88.8
$o\text{-}H_2D^+$	$p\text{-}H_2$	1.31(−10) 140.4	9.49(−11) 178.9	F	5.58(−10) 82.7	1.79(−9) −0.02	6.54(−10) 174.0
$o\text{-}H_2D^+$	$o\text{-}H_2$	4.67(−11) −0.82	1.64(−10) 6.31	8.31(−11) −0.92	1.68(−10) −0.77	2.19(−10) −0.72	1.14(−9) −0.06

3 H-2 D system

		$p\text{-}H_3^+$ $p\text{-}D_2$	$p\text{-}H_3^+$ $o\text{-}D_2$	$o\text{-}H_3^+$ $p\text{-}D_2$	$o\text{-}H_3^+$ $o\text{-}D_2$	$p\text{-}H_2D^+$ HD	$o\text{-}H_2D^+$ HD	$p\text{-}D_2H^+$ $p\text{-}H_2$	$p\text{-}D_2H^+$ $o\text{-}H_2$	$o\text{-}D_2H^+$ $p\text{-}H_2$	$o\text{-}D_2H^+$ $o\text{-}H_2$
$p\text{-}H_3^+$	$p\text{-}D_2$	2.21(−11) −0.20	F	F	F	3.50(−9) −0.41	5.08(−9) −0.08	3.02(−10) −0.12	4.08(−10) 0.62	F	F
$p\text{-}H_3^+$	$o\text{-}D_2$	F	1.73(−11) −0.29	F	F	3.06(−10) 0.59	2.42(−10) 0.08	F	F	4.81(−10) −0.42	5.39(−10) 0.06
$o\text{-}H_3^+$	$p\text{-}D_2$	F	F	3.14(−11) 0.29	F	F	8.02(−10) 0.09	F	7.50(−10) −0.10	F	F

TABLE VIII. (*Continued.*)

$o\text{-}H_3^+$	$o\text{-}D_2$	F	F	F	2.38(−11) −0.63	F	5.59(−10) 2.49	F	F	F	1.03(−9) −0.86	
$p\text{-}H_2D^+$	HD	7.83(−12) 237.8	9.48(−12) 146.6	F	F	2.08(−10) −0.50	2.84(−10) 88.5	4.12(−10) −0.50	1.89(−10) 33.1	7.32(−10) 0.30	1.93(−10) −0.64	
$o\text{-}H_2D^+$	HD	2.52(−12) 150.1	3.88(−12) 65.1	6.80(−12) 181.7	1.03(−10) 96.8	8.64(−11) −0.38	4.66(−10) 1.38	6.41(−11) 0.22	3.02(−10) −0.60	1.49(−10) −0.9	5.24(−10) −0.56	
$p\text{-}D_2H^+$	$p\text{-}H_2$	2.02(−10) 355.0	F	F	F	3.26(−10) 137.3	4.49(−10) 231.4	1.73(−9) −0.01	7.09(−10) 168.8	F	F	
$p\text{-}D_2H^+$	$o\text{-}H_2$	F	F	2.65(−11) 233.9	F	7.33(−11) 1.58	5.94(−10) 54.6	2.84(−10) −0.58	1.35(−9) −0.10	F	F	
$o\text{-}D_2H^+$	$p\text{-}H_2$	F	1.56(−11) 325.2	F	F	3.48(−10) 193.6	4.61(−10) 281.7	F	F	1.72(−9) −0.05	4.16(−10) 171.1	
$o\text{-}D_2H^+$	$o\text{-}H_2$	F	8.35(−12) 171.1	F	1.65(−11) 194.6	8.15(−11) 15.6	6.82(−10) 103.4	F	F	4.17(−10) −0.36	1.27(−9) −0.08	

2 H-3 D system

		$p\text{-}H_2D^+$ $p\text{-}D_2$	$p\text{-}H_2D^+$ $o\text{-}D_2$	$o\text{-}H_2D^+$ $p\text{-}D_2$	$o\text{-}H_2D^+$ $o\text{-}D_2$	$p\text{-}D_2H^+$ HD	$o\text{-}D_2H^+$ HD	$p\text{-}D_3^+$ $p\text{-}H_2$	$p\text{-}D_3^+$ $o\text{-}H_2$	$m\text{-}D_3^+$ $p\text{-}H_2$	$m\text{-}D_3^+$ $o\text{-}H_2$	$o\text{-}D_3^+$ $p\text{-}H_2$	$o\text{-}D_3^+$ $o\text{-}H_2$
$p\text{-}H_2D^+$	$p\text{-}D_2$	4.42(−11) −0.43	4.82(−11) −1.01	F	F	6.78(−10) −0.23	5.41(−10) 0.85	1.69(−11) −0.64	F	F	F	1.41(−10) −1.05	F
$p\text{-}H_2D^+$	$o\text{-}D_2$	2.07(−11) 86.3	7.62(−11) −0.65	F	F	2.57(−10) −0.55	7.49(−10) 0.60	F	F	2.27(−10) −0.86	F	1.60(−10) 0.11	F
$o\text{-}H_2D^+$	$p\text{-}D_2$	F	F	8.14(−11) 1.48	3.93(−11) 0.21	6.64(−10) 0.20	5.39(−10) −0.44	F	1.48(−11) −0.62	F	F	F	1.31(−10) 0.18
$o\text{-}H_2D^+$	$o\text{-}D_2$	F	F	3.95(−11) 88.5	8.52(−11) 1.73	2.74(−10) −0.36	8.75(−10) 0.53	F	F	F	1.63(−10) −1.57	F	8.01(−11) −0.94
$p\text{-}D_2H^+$	HD	1.54(−11) 145.5	1.17(−11) 57.0	9.47(−11) 237.3	4.68(−11) 146.2	6.53(−10) −0.73	3.36(−10) 1.80	1.45(−11) −0.69	4.09(−11) −0.71	F	F	1.09(−10) −0.78	3.70(−10) 0.52
$o\text{-}D_2H^+$	HD	7.83(−12) 202.2	2.12(−11) 107.6	3.59(−11) 285.1	7.79(−11) 196.7	2.90(−10) 48.3	7.54(−10) 0.04	F	F	1.36(−10) −0.15	2.07(−10) −0.10	1.10(−10) −0.27	2.84(−10) −0.38
$p\text{-}D_3^+$	$p\text{-}H_2$	2.21(−10) 379.2	F	F	F	1.77(−9) 225.2	F	1.69(−9) 0.00	F	F	F	F	F
$p\text{-}D_3^+$	$o\text{-}H_2$	F	F	3.00(−10) 286.7	F	1.69(−9) 52.3	F	F	1.59(−9) −0.41	F	F	F	F
$m\text{-}D_3^+$	$p\text{-}H_2$	F	1.65(−10) 344.9	F	F	F	9.57(−10) 239.3	F	F	1.69(−9) 0.00	F	F	F
$m\text{-}D_3^+$	$o\text{-}H_2$	F	F	F	1.90(−10) 262.7	F	1.53(−9) 65.6	F	F	F	1.68(−9) 0.00	F	F

TABLE VIII. (*Continued.*)

$o\text{-}D_3^+$	$p\text{-}H_2$	1.07(−10) 393.9	7.85(−11) 296.9	F	F	9.43(−10) 237.4	6.89(−10) 189.7	F	F	F	F	1.69(−9) 0.00	F
$o\text{-}D_3^+$	$o\text{-}H_2$	F	F	1.53(−10) 303.8	9.60(−11) 213.6	9.06(−10) 66.2	7.70(−10) 17.0	F	F	F	F	F	1.30(−9) −1.47

1 H-4 D system

		$p\text{-}D_2H^+$ $p\text{-}D_2$	$p\text{-}D_2H^+$ $o\text{-}D_2$	$o\text{-}D_2H^+$ $p\text{-}D_2$	$o\text{-}D_2H^+$ $o\text{-}D_2$	$p\text{-}D_3^+$ HD	$m\text{-}D_3^+$ HD	$o\text{-}D_3^+$ HD
$p\text{-}D_2H^+$	$p\text{-}D_2$	2.45(−10) −0.19	5.16(−11) 0.10	4.36(−11) 3.11	1.42(−10) 1.31	8.94(−11) −1.00	F	8.23(−10) −0.13
$p\text{-}D_2H^+$	$o\text{-}D_2$	3.74(−11) 85.9	1.62(−10) 0.29	1.05(−10) 35.6	9.12(−11) 3.65	7.44(−11) 0.11	2.93(−10) 0.16	7.59(−10) −0.52
$o\text{-}D_2H^+$	$p\text{-}D_2$	3.64(−11) 50.0	1.92(−10) −0.70	9.40(−11) −0.33	1.11(−10) −0.50	6.87(−11) −0.85	2.77(−10) −0.76	6.52(−10) 0.90
$o\text{-}D_2H^+$	$o\text{-}D_2$	5.75(−11) 137.7	7.31(−11) 50.3	4.28(−11) 85.5	2.24(−10) −0.85	F	5.82(−10) −0.08	5.81(−10) 0.40
$p\text{-}D_3^+$	HD	2.77(−10) 229.7	2.24(−10) 144.8	1.50(−10) 182.0	F	6.91(−10) 0.00	F	7.75(−10) 0.00
$m\text{-}D_3^+$	HD	F	1.08(−10) 206.7	8.74(−11) 251.3	2.65(−10) 154.3	F	1.41(−9) −0.25	5.97(−10) 46.3
$o\text{-}D_3^+$	HD	1.40(−10) 247.4	1.63(−10) 160.5	1.08(−10) 198.4	1.20(−10) 105.2	9.16(−11) 15.5	2.46(−10) −0.23	1.17(−9) −0.18

5 D system

		$p\text{-}D_3^+$ $p\text{-}D_2$	$p\text{-}D_3^+$ $o\text{-}D_2$	$m\text{-}D_3^+$ $p\text{-}D_2$	$m\text{-}D_3^+$ $o\text{-}D_2$	$o\text{-}D_3^+$ $p\text{-}D_2$	$o\text{-}D_3^+$ $o\text{-}D_2$
$p\text{-}D_3^+$	$p\text{-}D_2$	4.03(−10) −0.24	F	F	F	4.61(−10) −0.29	4.75(−10) 0.54
$p\text{-}D_3^+$	$o\text{-}D_2$	F	5.56(−10) −0.77	4.00(−10) 21.7	F	5.34(−10) 68.9	6.18(−10) −0.77
$m\text{-}D_3^+$	$p\text{-}D_2$	F	8.37(−11) −0.61	4.87(−10) −0.37	1.48(−10) −0.49	1.11(−10) 46.6	6.12(−10) 0.45
$m\text{-}D_3^+$	$o\text{-}D_2$	F	F	2.14(−10) 84.7	1.27(−9) −0.32	1.63(−10) 130.5	6.66(−10) 45.8
$o\text{-}D_3^+$	$p\text{-}D_2$	5.37(−11) 15.2	4.49(−11) −0.23	4.47(−11) −0.26	5.64(−11) 0.72	5.76(−10) −0.10	5.87(−10) −0.19
$o\text{-}D_3^+$	$o\text{-}D_2$	2.51(−11) 99.5	7.74(−11) 15.3	3.21(−10) 38.3	2.78(−10) −0.47	3.24(−10) 85.2	9.70(−10) −0.39

[1] G. Steigman, D. Romano, and M. Tosi, Mon. Not. R. Astron. Soc. **378**, 576 (2007).
[2] B. Parise, A. Castets, E. Herbst, E. Caux, C. Ceccarelli, I. Mukhopadhyay, and A. G. G. M. Tielens, Astron. Astrophys. **416**, 159 (2004).
[3] E. Roueff, D. C. Lis, F. F. S. van der Tak, M. Gerin, and P. F. Goldsmith, Astron. Astrophys. **438**, 585 (2005).
[4] A. G. G. M. Tielens, Astron. Astrophys. **119**, 177 (1983).
[5] B. Parise, C. Ceccarelli, A. G. G. M. Tielens, A. Castets, E. Caux, B. Lefloch, and S. Maret, Astron. Astrophys. **453**, 949 (2006).
[6] C. Ceccarelli, P. Caselli, E. Herbst, A. G. G. M. Tielens, and E. Caux, in *Protostars and Planets V*, edited by B. Reipurth, D. Jewitt, and K. Keil (University of Arizona Press, Tucson, 2007), pp. 47–62.
[7] R. Stark, F. van der Tak, and E. van Dishoeck, Astrophys. J. **521**, L67 (1999).
[8] P. Caselli, F. F. S. van der Tak, C. Ceccarelli, and A. Bacmann, Astron. Astrophys. **403**, L37 (2003).
[9] C. Vastel, T. Phillips, and H. Yoshida, Astrophys. J. **606**, L127 (2004).
[10] L. Pagani, M. Salez, and P. G. Wannier, Astron. Astrophys. **258**, 479 (1992).
[11] H. Roberts, E. Herbst, and T. J. Millar, Mon. Not. R. Astron. Soc. **336**, 283 (2002).
[12] H. Roberts, E. Herbst, and T. J. Millar, Astrophys. J. **591**, L41 (2003).
[13] H. Roberts, E. Herbst, and T. J. Millar, Astron. Astrophys. **424**, 905 (2004).
[14] C. Walmsley, D. R. Flower, and G. P. des Forêts, Astron. Astrophys. **418**, 1035 (2004).
[15] D. R. Flower, G. P. des Forêts, and C. Walmsley, Astron. Astrophys. **427**, 887 (2004).
[16] D. R. Flower, G. P. des Forêts, and C. M. Walmsley, Astron. Astrophys. **449**, 621 (2006).
[17] J. Le Bourlot, Astron. Astrophys. **242**, 235 (1991).
[18] D. Gerlich, E. Herbst, and E. Roueff, Planet. Space Sci. **50**, 1275 (2002).
[19] Y. Yamaguchi, J. F. Gaw, R. B. Remington, and H. F. Schaefer III, J. Chem. Phys. **86**, 5072 (1987).
[20] Z. Xie, B. J. Braams, and J. M. Bowman, J. Chem. Phys. **122**, 224307 (2005).
[21] P. H. Acioli, Z. Xie, B. J. Braams, and J. M. Bowman, J. Chem. Phys. **128**, 104318 (2008).
[22] G. M. e Silva, R. Gargano, W. B. da Silva, L. F. Roncaratti, and P. H. Acioli, Int. J. Quantum Chem. **108**, 2318 (2008).
[23] M. Barbatti and M. A. C. Nascimento, J. Chem. Phys. **119**, 5444 (2003).
[24] T. Oka and E. Epp, Astrophys. J. **613**, 349 (2004).
[25] K. Park and J. C. Light, J. Chem. Phys. **126**, 044305 (2007).
[26] M. Quack, Mol. Phys. **34**, 477 (1977).
[27] K. Park and J. C. Light, J. Chem. Phys. **127**, 224101 (2007).
[28] T. Oka, J. Mol. Spectrosc. **228**, 635 (2004).
[29] N. Adams and D. Smith, Astrophys. J. **248**, 373 (1981).
[30] K. Giles, N. Adams, and D. Smith, J. Phys. Chem. **96**, 7645 (1992).
[31] M. Cordonnier, D. Uy, R. M. Dickson, K. E. Kerr, Y. Zhang, and T. Oka, J. Chem. Phys. **113**, 3181 (2000).
[32] D. Gerlich, F. Windisch, P. Hlavenka, R. Plašil, and J. Glosik, Philos. Trans. R. Soc. London, Ser. A **364**, 3007 (2006).
[33] J. Ramanlal, O. Polyansky, and J. Tennyson, Astron. Astrophys. **406**, 383 (2003).
[34] J. Ramanlal and J. Tennyson, Mon. Not. R. Astron. Soc. **354**, 161 (2004).
[35] A. M. Messiah and O. W. Greenberg, Phys. Rev. **136**, B248 (1964).
[36] A.-W. Maue, Ann. Phys. **422**, 555 (1937).
[37] E. Hugo, O. Asvany, J. Harju, and S. Schlemmer, in *Molecules in Space and Laboratory* (S. Diana, Paris, edited by J. L. Lemaire and F. Combes 2007).
[38] L. Pagani, C. Vastel, E. Hugo, V. Kokoouline, C. Greene, A. Bacmann, E. Bayet, C. Ceccarelli, R. Peng, and S. Schlemmer, Astron. Astrophys. **494**, 623 (2009).
[39] C. M. Lindsay andB. J. McCall, J. Mol. Spectrosc. **210**, 60 (2001).
[40] J. Tennyson, personal communication (June, 2005).
[41] S. Miller and J. Tennyson, J. Mol. Spectrosc. **126**, 183 (1987).
[42] W. Kolos and L. Wolniewicz, J. Chem. Phys. **46**, 1426 (1967).
[43] D. Gerlich, J. Chem. Phys. **92**, 2377 (1990).
[44] W. H. Miller, J. Chem. Phys. **52**, 543 (1970).
[45] J. Hirschfelder, C. Curtiss, and R. Bird, *Molecular Theory of Gases and Liquids* (Wiley, New York, 1966), Chap. 2.1.
[46] E. I. Dashevskaya, I. Litvin, E. E. Nikitin, and J. Troe, J. Chem. Phys. **122**, 184311 (2005).
[47] T. Hill, *An Introduction to Statistical Thermodynamics* (Dover, New York, 1960).
[48] E. Herbst, Astron. Astrophys. **111**, 76 (1982).
[49] D. Gerlich, in *Adv. Chem. Phys.: State-Selected and State-to-State Ion-Molecule Reaction Dynamics*, edited by C.-Y. Ng and A. C. P. Michael Baer (Wiley, New York, 1992), Vol. LXXXII, pp. 1–176.
[50] D. Gerlich, Phys. Scr., T **T59**, 256 (1995).
[51] W. Paul, B. Lücke, S. Schlemmer, and D. Gerlich, Int. J. Mass Spectrom. Ion Process. **150**, 373 (1995).
[52] D. Gerlich, J. Chem. Soc., Faraday Trans. **89**, 2199 (1993).
[53] L. Amiaud, Ph.D. thesis, University of Cergy–Pontoise, 2006.
[54] O. Asvany, E. Hugo, F. Müller, F. Kühnemann, S. Schiller, J. Tennyson, and S. Schlemmer, J. Chem. Phys. **127**, 154317 (2007).
[55] O. Asvany, O. Ricken, H. S. P. Müller, M. C. Wiedner, T. F. Giesen, and S. Schlemmer, Phys. Rev. Lett. **100**, 233004 (2008).
[56] O. Asvany and S. Schlemmer, Int. J. Mass. Spectrom. **279**, 147 (2009).
[57] T. Wu, H. Werner, and U. Manthe, Science **306**, 2227 (2004).
[58] See EPAPS Document No. E-JCPSA6-130-032910 which includes (i) the equilibrium constants for all isotopic reaction up to 300 K, (ii) the partition functions of all nuclear spin symmetries of the H_3^+ and H_2^+ isotopologues up to 300 K and (iii) the complete set of state-to-state rate coefficients up to 50 K based on strong ergodicity and full-scrambling. For more information on EPAPS, see http://www.aip.org/pubservs/epaps.html.
[59] C. Vastel, P. Caselli, C. Ceccarelli, T. Phillips, M. C. Wiedner, R. Peng, M. Houde, and C. Dominik, Astrophys. J. **645**, 1198 (2006).